Cosmic Ray Physics Report

LUIP-CR-75-14

October 1975

INTERACTIONS OF 2 GeV/NUCLEON ^{16}O WITH LIGHT AND HEAVY EMULSION NUCLEI

B. Jakobsson and R. Kullberg

Department of Physics

University of Lund

Sölvegatan 14

S-223 62 LUND, Sweden

INTERACTIONS OF 2 GeV/NUCLEON ^{16}O WITH LIGHT AND HEAVY EMULSION NUCLEI

B. Jakobsson and R. Kullberg

Contents

Interactions of 2 GeV/Nucleon ^{16}O with Light and Heavy Emulsion Nuclei

B. Jakobsson and R. Kullberg

Department of Physics, University of Lund, Lund, Sweden.

Heavy ion interactions in nuclear emulsions induced by 2 GeV/nucleon ^{16}O have been studied. The reaction cross sections determined are 337^{+56}_{-85} mb, 1007^{+175}_{-174} mb and 2180^{+304}_{-231} mb for interactions with H, CNO and AgBr, respectively. Energy-, angular- and transverse momentum distributions of non-relativistic protons (E < 400 MeV) and all He nuclei have been analysed. Statistical models assuming small correlations among nucleon momenta can account for the main part of the He emission. The energy- and transverse momentum distributions of protons, emitted from light as well as heavy target nuclei indicate that intranuclear nucleon-nucleon scattering is the most important proton emission process. The angular distributions of both high energy protons and high energy He nuclei emitted from the target nucleus differ considerably in central and peripheral ^{16}O-AgBr interactions. In order to explain the angular distributions of high energy protons and He nuclei in events with extremely small impact parameter, non-statistical phenomena, possibly hydrodynamic shock wave emission, must be considered.

1. Introduction

The recent results of experiments using beams of heavy ions, accelerated in the Bevatron-Bevalac facility, have initiated an increased theoretical interest in the field of heavy ion interactions. Statistical models assuming minimal correlations

among nucleon momenta have been successful in describing momentum distributions of relativistic fragments in peripheral interactions [1,2]. In these models, the reactions are often assumed to take place in two steps, a fast step where a few nucleons in the overlap region of the nuclei are removed, and a slower step where an excited residual nucleus is deexcited by particle emission. An intermediate reaction step, which has been included in the abrasion-ablation model, accounts for reabsorption of nucleons emitted in the fast (abrasion) step [3]. In order to predict fragmentation cross sections and investigate the validity of the factorization hypothesis, multiple scattering calculations, using the Glauber theory, have been extended to heavy ion reactions [4-6].

Large deviations from the above-mentioned models have been reported for interactions with small impact parameter [7,8]. In Ref. 7 it is shown that the pion production in nucleus-nucleus interactions with a complete breakup of the target nucleus can hardly be reproduced unless several nucleons interact in a cooperative fashion. It has lately been proposed that shock wave propagation should appear in central heavy ion reactions. The shock wave thereby initiates density perturbations causing particle emission from the nuclear surface [9-11].

In this report we present results from ^{16}O reactions at 2 GeV/ /nucleon in hydrogen, light nuclei (C,N,O) and heavy nuclei (Ag,Br). In the investigation we used a low sensitive emulsion type (Ilford K2). Therefore we could determine the charge of light particles even with short ranges, which is important for the identification of the target nuclei in the emulsion. Furthermore, we found that a track of a particle with range < 10 μm

and a charge ≥ 3 is almost exclusively associated with an Ag or Br target nucleus. Consequently, a distinct separation between interactions in the three target groups H, CNO and AgBr was possible to obtain. The experimental reaction cross sections of ^{16}O-H, -CNO and -AgBr interactions agree with predictions from multiple scattering calculations. Owing to the high precision in the target determination and the wide energy intervals in which protons and He nuclei could be identified we have been able to present complete energy-, angular- and transverse momentum distributions of non-relativistic light particles.

2. Experimental Details

2.1. Emulsion Stack and Exposure

The emulsion stack consisted of 17 Ilford K2 pellicles, 600 μm thick and 10x10 cm^2 in size. The stack was exposed with the emulsion plane parallel to the 2.1 GeV/nucleon ^{16}O beam of the Berkeley Bevatron. The flux was 2.6×10^4 ions/cm^2. A temperature development method with a dry hot stage (20°C) and a hypo-stage (10°C) was used. The sensitivity of the emulsions was found to be high enough to give visible tracks of relativistic singly charged particles (6.6 grains per 100 μm).

2.2. Scanning

A total volume of 0.18 cm^3 in three plates in the middle of the stack was area-scanned three times by three different scanners using 275x magnification. The second re-scan gave an additional number of events < 2 %. 269 events were found and analysed.

2.3. Particle Identification

To identify particles in the emulsion we have to use measurable

parameters associated with the energy loss. In this experiment the gap density, the total blob length and the gap length distribution of tracks were used. These parameters are associated with the track core. Consequently, we have taken the energy loss of charged particles restricted to the track core (REL) as the theoretical counterpart of the measured parameters [12]. We have thereby assumed that electrons with a kinetic energy above 2 keV do not contribute to the blackness of the track core.

Charge identification of relativistic multiply charged fragments was made by measurements of the gap density, (He,Li) or the frequency of gaps with a length > 3 μm, at the star and in at least one point more than 2 cm from the star (Table 1).

Table 1. Energy loss parameters of relativistic multiply charged particles

	He	Li	Be	B	C	N	O
Gap density $(100\ \mu m)^{-1}$	23.6	44.1	54.9	56.7	56.3	56.1	54.2
N(>3 μm) $(100\ \mu m)^{-1}$	11.3	6.0	4.8	2.8	1.4	0.73	0.37

N(> 3 μm) = The number of gaps with a length > 3 μm.

The gap density values in Table 1 have been obtained from the gap density-REL calibration curve in Fig. 1. This curve was obtained by using pions and protons with small dip angles and with ranges long enough to make the identification from the rate of change of REL safe. Since one side of the emulsion stack has been exposed to a 250 MeV/nucleon ^{20}Ne beam, we could extend

the calibration curve to several hundred MeV/cm by measuring the gap density of Ne tracks stopping in the stack.

The statistical error of the gap density is for a He track ~ 4 % and for an ^{16}O-track ~ 2 % when measuring on a track length of 2 mm. From Table 1 we notice that only He and Li could be identified by gap density measurements. The gap length coefficient (g, discussed in Appendix 1) was determined for ^{16}O tracks from the beam and for H-, He- and Li fragments. These g values were used to calculate the frequency of gaps with a length > 3 μm shown in Table 1. N(> 3 μm) was measured in 1 cm of the relativistic fragments in order to get charge separation. These fragments were also easily separated from low energy particles according to Ref. 13.

For all non-relativistic tracks gap density measurements were performed near the star. Tracks with a dip angle $\leq 40^{\circ}$ were followed until they stopped or left the stack. The gap density of these tracks was measured in at least one other point if the range (R) exceeded 2 mm. A dip angle correction of the gap density according to Appendix 1, has been introduced. The total blob length (TBL) of the last 50 and 95 μm was also determined for tracks stopping in the emulsion stack. Thereby the coordinate of the beginning and the end of every blob was measured along the track projected in the emulsion plane and referred to the point where the particle stopped. The measured TBL values have been corrected for the dip angle analogous to the gap density correction (Appendix 1).

The TBL distribution of the last 95 μm is shown in Fig. 2. Calibration tracks of long range protons, deuterons, helium- and

lithium nuclei, identified by gap density measurements, are specially marked. We have taken the minimum in the distribution at 79 μm as the limit between hydrogen- and He nuclei, and the minimum at 89.5 μm as the limit between He- and heavier nuclei. With these criteria all calibration tracks fall into the correct groups. However, it is quite obvious that isotopic resolution is not to be expected from the TBL measurements. For all particles with $R > 95$ μm we have studied TBL as a function of the residual range in the interval $0 \leq R \leq 95$ μm. By using the behaviour of the identified particles, we could extend the separation between hydrogen-, helium and heavier nuclei to most particles with $R < 95$ μm.

2.4. Angular and Energy Measurements

Emission angles (θ) and dip angles (φ) of all particles were determined by measuring coordinates of the interaction centre and of points on the incident and secondary tracks near the star. The coordinate normal to the emulsion plane was corrected for the reduction of the thickness of the emulsion during the processing. This reduction was determined by measuring the emulsion thickness before and after the processing.

For relativistic fragments coordinates were measured in four points along the fragment track as well as along the projectile track. Least square fits of straight lines to the coordinates in the planes parallel with and normal to the emulsion plane were performed to receive small errors in the emission angles. No significant difference in the mean displacements of the track in these two planes were found. With this method the error of the angle should not exceed 3 mr in any case.

3. The Isotopic Composition of the Hydrogen Nuclei

In this section we discuss the amount of deuterons and tritons among the hydrogen nuclei. For this purpose the relation between TBL and residual range (R) for protons in the interval $0 \leq R \leq 100$ μm was determined from 64 calibration protons with a total range > 4 mm and a dip angle $\leq 30^{\circ}$ (Fig. 3). The TBL-R relations for deuterons and tritons have been calcuiated from the velocity-range formula below [12,14,15] and the experimental TBL-R relation for protons. The formula used is:

$$R = \frac{M}{Z^2} \left(\lambda(\beta) + B_Z(\beta)\right) \qquad (1)$$

where $B_Z(\beta) = \begin{cases} 1.525 \cdot 10^{-3} \cdot \beta \cdot Z^{5/3} \text{ (cm)} & \text{if } \beta \leq 0.0146 \cdot Z \\ 2.333 \cdot 10^{-5} \cdot Z^{8/3} \text{ (cm)} & \text{if } \beta \geq 0.0146 \cdot Z \end{cases}$

$\lambda(\beta)$ is the range of an ideal proton,

M is the mass and Z is the charge of the nucleus.

From Fig. 3 we find that <TBL> = 70.3 μm for the last 95 μm of a proton track. A rough way of estimating the number of protons is to adapt a Gaussian curve with this mean value to the experimental TBL distribution below 69 μm, where the admixture of heavy isotopes is expected to be small. This Gaussian is shown in Fig. 2 (solid curve). If we now subtract the proton Gaussian from the experimental TBL distribution we can repeat the same procedure to derive a deuteron Gaussian (the deuteron Gaussian is fitted in the interval $65 \leq TBL \leq 72$ μm). Finally, a triton distribution has been estimated in the same way (the triton Gaussian is fitted in the interval $70 \leq TBL \leq 74$ μm). The total p+d+t distribution estimated in this way is shown by the dashed curve in Fig. 2. This curve justifies the use of 79 μm as the limit between hydrogen- and He nuclei.

The d+t contribution to hydrogen nuclei from the above estimation is ~ 38 %. This value is valid for hydrogen tracks in a range interval corresponding to the energy intervals 3.4 - 52 MeV for protons, 4.3 - 70 MeV for deuterons and 4.8 - 83 MeV for tritons. In Ref. 16 the amount of heavy hydrogen isotopes is found to be 33 % for proton-Ag interactions at 5.5 GeV. In the proton-Ag experiment, protons with E < 28 MeV, deuterons with E < 32 MeV and tritons with E < 42 MeV are included.

4. Short Range Tracks and Target Identification

4.1. Introductory Remarks

In interactions with emulsion nuclei we can divide the targets into three groups: H, CNO and AgBr. A rough target separation into these groups can be made by using the number of charged particles with $\beta<0.7$ (N_h). Stars with $N_h \geq 8$ are considered to be collisions with AgBr, whereas stars with $N_h \leq 1$ are regarded as H events. In Ref. 17 we showed that the accuracy of this identification method increases with increasing charge of the incident nucleus. However, for ^{16}O interactions less than 75 % of the AgBr events can be identified by the simple criterion $N_h \geq 8$. In order to identify the rest of the AgBr events we have to use the information which can be obtained from short range tracks.

Generally, we observe no gaps on the last 10 μm of tracks from particles with $Z \geq 3$. On the other hand, both tracks of protons and He nuclei (Fig. 3) usually have visible gaps even for ranges less than 10 μm, due to the low sensitivity of K2 emulsions. Thus we were able to make a rough separation between H+He and $Z \geq 3$ particles with R < 50 μm.

4.2. Target Identification

For proton-emulsion nucleus interactions Barashenkov et al. [18] have suggested that AgBr events with $N_h < 8$ must fulfil the following criteria:

i) At least one track with $R \leq 10$ μm should be found.

ii) No tracks with $10 < R \leq 50$ μm should be found.

In our investigation we have determined the charge of most low energy particles. Therefore we estimate the lower limit of the charge carried away from the target nucleus (ΔZ_{min}) instead of N_h. A larger part of the AgBr events is directly identified if the criterion $\Delta Z_{min} > 8$ is used instead of the criterion $N_h \geq 8$. ΔZ_{min} is given by the formula:

$$\Delta Z_{min} = N_p + 2N_{He} + 3N_{Z\geq 3} + N_{\varphi>40} + \Sigma Z_i \qquad (2)$$

N_p = The number of identified slow ($\beta<0.7$) hydrogen nuclei

N_{He} = -"- -"- -"- He nuclei

$N_{Z\geq 3}$ = -"- -"- -"- $Z\geq 3$ nuclei

$N_{\varphi>40}$ = The number of tracks with $\varphi > 40^0$ and $R > 50$ μm

Z_i = The estimated charge of a track with $R < 50$ μm ($Z_i = 1$, 2 or 3).

The range distribution of H+He and $Z \geq 3$ nuclei, in the interval $0 \leq R \leq 50$ μm, for events in different ΔZ_{min} intervals are shown in Fig. 4. The following observations of importance for the target determination can be made from these range distributions.

i) The frequency of heavy particles is large only for $R \leq 10$ μm whereas the light particles are distributed over the whole range interval, $0 \leq R \leq 50$ μm.

ii) The frequency of heavy particles increases significantly

with decreasing ΔZ_{min} in AgBr events ($\Delta Z_{min} > 8$). However, this frequency decreases in events with $2 \leq \Delta Z_{min} \leq 8$.

iii) The frequency of light particles (H+He) decreases with decreasing ΔZ_{min} in AgBr events ($\Delta Z_{min} > 8$). In contradiction to heavy particles, the frequency of light particles increases in events with $2 \leq \Delta Z_{min} \leq 8$.

These observations indicate that the Coulomb barrier is high enough to depress the emission of low energy light particles only in peripheral collisions with a heavy target nucleus. It is therefore reasonable to assume that the large number of low range $Z \geq 3$ particles in peripheral collisions are recoil nuclei, instead of particles emitted through the Coulomb barrier. This assumption is further established in Chapter 5, where we also conclude that most short range $Z \geq 3$ particles in events with $\Delta Z_{min} \leq 8$ are recoil nuclei from interactions in Ag or Br. The importance of short range particles for the target separation is further pronounced by Fig. 5. In this figure we show the relation between ΔZ_{min} and the frequency of events in which light particles with $R < 50$ μm but no heavy short range particles are emitted. The structure of this curve clearly shows that in peripheral AgBr events we cannot expect light particles to be emitted if no heavy particles are emitted as well. The dramatic increase in the frequency for $\Delta Z_{min} < 8$ is obviously due to CNO events.

The above results have been used to identify target nuclei according to the following criteria:

AgBr events: 1. $\Delta Z_{min} > 8$.

2. $\Delta Z_{min} \leq 8$ and at least one track with $Z \geq 3$ and $R \leq 10$ μm is present.

CNO events: $2 \leq \Delta Z_{min} \leq 8$ and no track with $Z \geq 3$ and $R \leq 10$ μm is present.

H events: $\Delta Z_{min} \leq 1$.

These criteria give $51.3^{+6.6}_{-4.4}$ % AgBr events, 37.9 ± 6.0 % CNO-events and $10.8^{+2.0}_{-4.2}$ % H events. The total errors include a statistical error as well as the probability of making wrong target identifications due to the approximation that all particles with $\varphi > 40^{\circ}$ have been assigned a charge of 1.

5. Recoil Nuclei

In the previous section we suggested that most particles with $Z \geq 3$ and $R \leq 10$ μm are recoil nuclei. In this chapter we investigate whether the range distributions of these particles (Fig. 4) are in agreement with the recoil nucleus assumption. Therefore we start by making an estimation of the velocity of recoil nuclei and then we determine the corresponding ranges in emulsion for ions with different masses. If the protons are emitted isotropically from an excited recoil nucleus the following formulas are valid:

$$p^* \cos\theta^* = p \cos\theta - mc\beta_{\parallel} \qquad (3)$$

$$\langle p^* \cos\theta^* \rangle = 0$$

where p and θ are the momentum and the emission angle in the laboratory frame,

p^* and θ^* are the momentum and the emission angle in the rest system of the recoil nucleus and

m is the proton mass.

In the energy interval $4 \leq E^* \leq 25$ MeV, we have studied

$\langle p^* \cos\theta^* \rangle$ as a function of $\beta_{\parallel}$ in different kinds of events. The lower energy limit is chosen in order to exclude all protons with R < 50 μm which are not safely identified. The upper limit is chosen in order to minimize the effect of protons emitted from non-isotropic processes. Fits of linear relations between $\langle p^* \cos\theta^* \rangle$ and $\beta_{\parallel}$ for small $|\langle p^* \cos\theta^* \rangle|$ were performed. Thereby, we obtain the $\langle \beta_{\parallel} \rangle$ values in Table 2, for $\langle p^* \cos\theta^* \rangle = 0$.

Table 2. $\langle \beta_{\parallel} \rangle$ of the recoil nucleus in different kinds of events.

Event	$\langle \beta_{\parallel} \rangle$	
	$4 \leq E^* \leq 25$ MeV	$E^* \leq 25$ MeV
AgBr, $\Delta Z_{min} \leq 8$	0.012 ± 0.003	0.009 ± 0.005
AgBr, $9 \leq \Delta Z_{min} \leq 17$	0.012 ± 0.002	0.014 ± 0.002
AgBr, $\Delta Z_{min} \geq 18$	0.024 ± 0.001	0.022 ± 0.001
AgBr total	0.019 ± 0.001	0.019 ± 0.001
CNO total	0.002 ± 0.005	0.003 ± 0.003

We have also calculated $\langle \beta_{\parallel} \rangle$ when the low range particles (R < 50 μm), estimated as protons, are included, However, this does not change the $\langle \beta_{\parallel} \rangle$ values very much.

There is a significant increase of $\langle \beta_{\parallel} \rangle$ in AgBr events with increasing target disintegration. The recoil velocity of light target nuclei is very small and even significantly smaller than the velocity in peripheral AgBr events. The same tendencies have been shown at lower incident energies in Ref. 19.

In order to estimate $\langle \beta_{\perp} \rangle$ we have used protons in the energy in-

terval $4 \leq E \leq 25$ MeV. The mean value of p_x, p_y and p_z for these protons was determined for each event ($\langle p_x \rangle$, $\langle p_y \rangle$, $\langle p_z \rangle$). For each group of events in Table 2 we then determined the mean values of $|\langle p_x \rangle|$, $|\langle p_y \rangle|$ and $|\langle p_z \rangle|$. Thereby, we found that the mean transverse momentum is $\approx |\langle p_x \rangle|$ for all groups of events.

We have therefore assumed the mean velocity of recoil nuclei to be $\sqrt{2} \langle \beta_{\perp} \rangle c$. Ranges in emulsion of recoil nuclei with β values corresponding to the $\langle \beta_{\perp} \rangle$ values in Table 2 are shown in Table 3. At these low velocities the effective charge of the ion is very much reduced owing to charge pick up. The ranges which are presented in Table 3 have been derived from formula (1).

This formula is based on experimental ranges of ions with $M \leq 40$ [14]. We have, however, used the same formula also for ^{60}Ni and ^{80}Br. The LSS energy-range theory [20], which is valid for these heavy ions according to experiments of Bowman et al. [21], gives ranges which differ less than ± 2 μm from the values in Table 3.

Table 3. Estimated range in emulsion of nuclei with different velocities.

Nucleus	Range (μm)			
	$\beta = 0.004$	$\beta = 0.013$	$\beta = 0.020$	$\beta = 0.031$
$^{80}_{35}$Br	2	5	8	12
$^{60}_{28}$Ni	1	4	6	10
$^{16}_{8}$O	0.5	2	3	5
$^{7}_{3}$Li	0.5	2	3	6

The nuclei ^{80}Br, ^{60}Ni and ^{16}O have been selected in order to choose typical recoil nuclei from AgBr events with $\Delta Z_{min} \leq 8$, $9 \leq \Delta Z_{min} \leq 17$ and $\Delta Z_{min} \geq 18$, respectively.

The following conclusions can be drawn from the comparison between the range distributions of particles with $Z \geq 3$ in Fig. 4 and the velocity- and range calculations (Tables 2 and 3) of recoil nuclei.

i) The experimental range distribution of heavy particles in central AgBr events ($\Delta Z_{min} \geq 18$) cannot be completely explained by the expected range distribution of light recoil nuclei ($Z \sim 8$) with velocities around 0.03c. It is, however, likely that some of these particles are light fragments emitted with low energies from a nucleus with strongly reduced Coulomb barrier [22].

ii) The experimental distribution of heavy particles in peripheral AgBr events ($9 \leq \Delta Z_{min} \leq 17$) is in agreement with the expected range distribution of heavy recoil nuclei with velocities distributed around 0.02c.

iii) The range distribution of heavy particles in the ΔZ_{min} interval 2-8 cannot be explained neither by recoil nuclei from CNO events nor by emitted fragments from CNO events. This conclusion can be drawn from a) the range estimations in Table 3 and b) from the fact that ranges expected from the experimental momentum distributions of relativistic fragments in reactions between ^{16}O and ^{10}Be at 2.1 GeV/nucleon [23] are almost exclusively < 3 μm. On the contrary, the expected range distribution of heavy recoil nuclei from peripheral AgBr events (velocities around 0.01 c) is in agreement with the experimental range distribution.

These results strongly indicate, that events with $2 \leq \Delta Z_{min} \leq 8$

which include tracks of particles with $Z \geq 3$ and $R < 10$ μm are AgBr events.

6. Reaction Cross Sections

6.1. Experimental Cross Sections

The scanning efficiency was almost 100 % for events in which either

i) the difference between the charges of the beam and the heaviest relativistic fragment $\Delta Z \geq 4$ or

ii) the number of heavy prongs, $N_h \geq 2$.

The reaction cross sections have been corrected for the scanning loss of events with $\Delta Z \leq 3$ by using the isotopic production cross sections given by Lindstrom et al. [24]. The mean free path in emulsion, thus determined, is 12.3 ± 1.3 cm in agreement with results given in Refs. 25 and 26.

The target identification described in the previous section, the standard emulsion composition [12] and the above-mentioned corrections for events with $\Delta Z \leq 3$ give the reaction cross sections shown in Table 4. The errors include the uncertainty in

Table 4. Reaction cross sections for ^{16}O-H, -CNO, -AgBr and -emulsion interactions (mb).

	σ_H	σ_{CNO}	σ_{AgBr}	$\sigma_{emulsion}$
This experiment	337^{+56}_{-85}	1007^{+175}_{-174}	2180^{+304}_{-231}	1033±108
Barshay et al. [4]	340	1130	2600	1180
Fäldt and Gislén [6]	335	995	2476	1104

the target determination (chapter 4.2). The experimental cross sections are in good agreement with theoretical calculations.

Barshay et al. [4] use a geometrical description of the nuclei and the cross sections are calculated with an impact parameter representation of the scattering amplitude. Fäldt and Gislén [6] describe the incident ^{16}O nucleus with an alpha particle model, where each alpha particle is assumed to have a Gaussian density distribution. The cross sections are then calculated by multiple scattering theory.

6.2. Cross Sections in the Bradt-Peters Formalism

A useful geometrical expression of heavy ion reaction cross sections, at least in a limited energy region, is the Bradt-Peters formula:

$$\sigma_R = \pi r_o^2 (A_B^{1/3} + A_T^{1/3} - b)^2 \qquad (4)$$

where A_B and A_T are the mass numbers of beam and target nucleus respectively and

b is the geometrical overlap divided by r_o.

Recently it has been suggested that the parameters r_o and b depend on the size of the interacting nuclei [25]. In Fig. 6 we have plotted the overlap parameter, b, as a function of $A_B^{1/3} + A_T^{1/3}$ for all heavy ion reaction cross sections known to us [27-29, this work], under the approximation that $r_o = 1.25$ fm for all nuclei. In addition some nucleon-nucleus reaction cross sections in the GeV region have been included in Fig. 6 [30-32].

It has been suggested that b only depends on the smallest mass number of the interacting nuclei [27]. The limited present data concerning reactions induced by nuclei with $Z \geq 2$ would rather seem to imply that one single linear relation between b and $(A_B^{1/3} + A_T^{1/3})$ may be used to predict all heavy ion reaction cross sections. The overlap formula (4) with:

$$r_o = 1.25 \text{ fm}$$
$$b = -0.20\ (A_B^{1/3} + A_T^{1/3}) + 1.56 \qquad (5)$$

(under the assumption that all experimental points have the same weight) fits all the experimental heavy ion cross sections to within 15 %.

It is obvious that the linear relation between b and $(A_B^{1/3} + A_T^{1/3})$ cannot account for the nucleon-nucleus cross sections. It must, however, be noticed, that the experimental reaction cross sections of nucleus-hydrogen interactions are significantly larger than corresponding nucleon-nucleus cross sections. In fact all the nucleus-hydrogen cross sections are well accounted for by the overlap formula given above.

7. Characteristics of the Emission of Protons, He- and Li Nuclei

7.1. Remarks about the Experimental Energy- and Angular Distributions

In this experiment deuterons and tritons could be separated from protons only if $R \geq 4$ mm. However, we found no significant difference in the angular distribution between hydrogen tracks with small and with large TBL values. Subsequently, we have treated all hydrogen nuclei as protons. In the $d\sigma/dE$ distribution this

approximation has been taken into consideration in the horizontal errors.

All He nuclei have been treated as alpha particles. The errors introduced by this approximation are negligible since the range has been measured for all He nuclei except two, and the energy difference between ^{3}He- and ^{4}He nuclei with tne same range is < 10 %.

Particles with dip angle > 40° have not been identified and a geometrical correction is therefore introduced. The weight for particles with emission angles in the interval $40^\circ \leq \theta \leq 140^\circ$ is:

$$W(\theta) = 90/\arcsin(\sin 40^\circ/\sin\theta) \qquad (6)$$

This formula is derived in Appendix 2.

7.2. Energy Distributions

Fig. 7 shows the differential cross sections summarized over all emission angles ($d\sigma/dE$) as a function of the total kinetic energy. In Fig. 7a we compare $d\sigma/dE$ for protons emitted in AgBr and CNO events and a corresponding comparison for He nuclei is shown in Fig. 7b. In AgBr events the energy spectra of protons and He nuclei below ~ 30 MeV follow the characteristic exponential shapes of evaporation spectra. At energies larger than ~ 50 MeV, the shape of the proton spectra are well accounted for by simple intranuclear cascade calculations. This is demonstrated in Fig. 7a by the curves, which are results of cascade calculations in proton-nucleus interactions at 1840 MeV (33). The agreement between these calculations and our experimental energy distributions of protons indicates that intranuclear nucleon-nucleon scattering may be responsible for a dominant part of the emitted protons above 50 MeV in nucleus-nucleus interactions. Neither the Fermi

motion of nucleons in the incident ^{16}O nucleus nor the difference between the relative number of first encounters in nucleon-nucleus and nucleus-nucleus interactions, can change the main characteristics of the scattering spectra.

The frequency of He nuclei with E > 50 MeV is negligible in CNO events in comparison with the frequency in AgBr events. The high energy part of the $d\sigma/dE$ distribution of the emitted He nuclei in AgBr events has a power law form $\sim E^{-\alpha}$. We have fitted power laws to our He and Li spectra for $E \geq 40$ MeV and $E \geq 100$ MeV by the method of least squares. The exponents α are within the limits of error the same for both energy intervals. In Table 5 we compare the exponent with that obtained in other reaction types.

Table 5. The exponent α of the energy distribution ($d\sigma/dE \sim E^{-\alpha}$) of He nuclei in different reaction types. E > 100 MeV.

Reaction	Incident energy	Fragment	α	Reference
^{16}O-AgBr	2.0 GeV/n	He	2.5±0.3	This work
^{16}O-AgBr	2.0 GeV/n	Li	~ 2.5	This work
^{12}C-Au	2.1 GeV/n	B	~ 2.7	34
^{12}C-Au	2.1 GeV/n	O	~ 5	34
$^{<40>}_{<19>}X$-AgBr	> 1 GeV/n	He	1.8±0.1	17
π-AgBr	7.5 GeV	He	3.0±0.4	35
p-AgBr	2.3 and 9 GeV	He	3.3±0.3	35

The α values indicate that the steepness of the energy spectra of He nuclei decreases with increasing mass of the incident particle.

The value of α for nucleon-He elastic scattering is ~ 7 [17] and neither secondary intranuclear collisions nor Fermi motion of nucleons can reduce the α value with a factor 3. A large part of the high energy He nuclei are emitted with large angles. This is a further evidence that other processes than quasi-elastic scattering must occur.

It could also be noticed here that the dominant part of the high energy He nuclei (E > 40 MeV) are emitted in events with a large degree of target disintegration (~ 65 % in events with $N_h \geq 20$). A further discussion of these head on events is found in Chapter 8.

7.3. Angular Distributions

In the energy interval E $\leq$ 40 MeV angular distributions of protons, He- and Li nuclei from CNO as well as AgBr events can all be explained by an isotropic emission from a system moving in the forward direction with velocities < 0.03c. In Fig. 8 the differential cross sections, $d\sigma/d\Omega$, for protons with E > 40 MeV in AgBr and CNO events are compared. Fig. 9 shows $d\sigma/d\Omega$ for protons, He- and Li nuclei (E > 40 MeV) emitted in AgBr events. The results which could be pointed out from the angular distributions are:

i) An exponential distribution, $d\sigma/d\Omega \sim \exp(-\text{const}\cdot\theta)$, describes the gross features of the proton emission both in AgBr and CNO events. It should, however, be noticed that these smooth curves are not reproduced if only head on- or only peripheral events are regarded (chapter 8).

ii) The angular spectra of high energy fragments from a heavy target nucleus show an increasing isotropy with increasing fragment mass.

7.4. Transverse Momentum Distributions of He Nuclei

In an earlier article (13), we have reported on transverse momentum distributions of relativistic multiply charged fragments from the incident ^{16}O nucleus. The distribution:

$$N(p_\perp) \sim p_\perp \exp(-p_\perp^2/2\sigma^2) , \qquad \sigma \approx 140 \text{ MeV/c} \qquad (7)$$

describes the main structure of the fragment emission. This expression is derived if two independent Gaussian distributions of the transverse momentum components are applied. This is in agreement with results found by Greiner et al. [23]. However, we observed deviations from this picture especially for light fragments (He and Li), where the experimental distributions are extended to much larger $p_\perp$ values than the composite Gaussian distribution can account for. In another report Judek [26] has confirmed our results and found that the largest $p_\perp$ values appear in interactions with large meson production and a large target disintegration.

In Fig. 10 we present the experimental transverse momentum distributions of He nuclei emitted from the projectile as well as from the target nucleus. The histograms show that the $p_\perp$ distribution of projectile He has a weak dependence on the mass of the target nucleus. For events where ^{16}O interacts with a hydrogen nucleus the distribution is very well described by the composite Gaussian momentum distribution with $\sigma \approx 140$ MeV/c. The main features of the $p_\perp$ distributions in CNO and AgBr events are also described by this distribution. However, there is a small excess of particles with large $p_\perp$ values in the experimental distributions, which increases slightly with increasing target mass. This excess is connected with the increasing cross

sections of fragmentation channels where only one He nucleus is emitted from the ^{16}O beam nucleus. According to Refs. 13 and 26 these emission channels lead to wide $p_\perp$ spectra of He nuclei.

In ^{16}O-CNO reactions we are close to symmetry in the centre of mass system. Furthermore ~ 90 % of the target nuclei have a four-nucleon configuration (^{12}C, ^{16}O).. Therefore, we expect the $p_\perp$ spectra of He nuclei emitted from the incident nucleus and the target nucleus to be almost identical. This agreement is clearly demonstrated by Fig. 10 and by the frequencies of He nuclei given in Table 6. A comparison between curve 1 (target-He, CNO events) and curve 2 (target-He, AgBr events), clearly shows that the extension to larger $p_\perp$ values of He nuclei increases with increasing mass of the emitting nucleus.

Table 6. The frequency of He nuclei in ^{16}O-H, -CNO and -AgBr reactions.

	Number of He nuclei per interaction		Number of He nuclei with $p_\perp$>120 MeV/c per nucleon and per interaction*	
projectile He:	This work	Lindstrom et al. [24]	This work	Composite Gaussian
^{16}O-H	1.06 ± 0.16	0.80±0.12	0.05±0.04	0.002
^{16}O-CNO	0.78 ± 0.09	0.63±0.07**	0.08±0.03	0.001
^{16}O-AgBr	0.50 ± 0.05	0.46±0.06**	0.11±0.03	0.001
target He:				
^{16}O-CNO	0.85 ± 0.10	-	0.02	-
^{16}O-AgBr	2.68 ± 0.15	-	0.63±0.08	-

* The limit 120 MeV/c per nucleon is chosen in order to exclude He nuclei emitted with an energy < 30 MeV.

** For N, O and Br targets the He production cross sections are estimated from the formula $\sigma_{BT}^F = \gamma_B^F \cdot \gamma_T$ [24].

Table 6 shows that the frequency of He nuclei from the ^{16}O beam nucleus decreases with increasing target mass in agreement with results found in Ref. 17. The decrease in the He frequency is approximately $\sim A_T^{\frac{1}{3}}/\sigma_R$, which is expected if a strict factorisation of the fragmentation cross section is valid ($\sigma_{BT}^F = \gamma_B^F \cdot \gamma_T$ and $\gamma_T = A_T^{\frac{1}{3}}$). The frequencies from this experiment have been compared to the frequencies which can be estimated from spectrometer measurements in Berkeley [24]. We find in our experiment slightly larger frequencies of He nuclei. This excess can be explained by He nuclei with large $p_\perp$ values, which are not taken into consideration if a composite Gaussian distribution is extrapolated to large $p_\perp$ values. This statement is evident from the difference in frequency of He nuclei with $p_\perp >$ > 120 MeV/c per nucleon (Table 6) between the composite Gaussian prediction ($\sigma \approx 140$ MeV/c) and our experiment.

7.5. Transverse Momentum Distributions of Protons

The $p_\perp$ distributions of protons from CNO and AgBr events (Fig. 11) have a non-Gaussian shape. Included in Fig. 11 is the distribution which should be valid if each momentum component has a Gaussian shape ($\sim\exp(-p_x^2/2\sigma^2)$) and σ has the parabolic form expected from statistical models with small correlations among nucleon momenta [2]:

$$\sigma^2 \approx \sigma_o^2 A_F (A_B - A_F)/(A_B - 1) \qquad (8)$$

where A_F is the fragment mass number and

A_B is the beam mass number.

From experiments on peripheral heavy ion reactions σ_o values between 70 and 90 MeV/c have been suggested [2,23].

This statistical model is not valid for non-peripheral collisions. However, in our experimental sample the dominant part of the protons are in fact emitted in non-peripheral collisions, where intranuclear nucleon-nucleon scattering is important (section 7.2). Thus it is not surprising that the experimental $p_\perp$ distribution is much wider than the distribution predicted by the statistical models.

8. Particle Emission from Heavy Nuclei in Interactions with Small Impact Parameter

In recent studies, it has been observed that strange phenomena in meson-, proton- and alpha emission occur in nucleus-nucleus interactions with a total disintegration of a heavy target nucleus [7,8]. By using the ordinary criterion of a total disintegration of an Ag or Br nucleus into protons and He nuclei, $N_h \geq 28$, [17] we can study events with an extremely small impact parameter. We noticed in the previous chapter that the gross features of the energy- and angular distributions of protons emitted in all AgBr events could be accounted for by intranuclear nucleon-nucleon scattering and evaporation.

In Fig. 12 we present the angular spectrum of protons in events with $N_h \geq 28$. The structure of this distribution deviates significantly from the angular distribution of protons emitted in all AgBr events (Fig. 8) and also from what could be expected if nucleon-nucleon scattering had been the only emission process. The following deviations from the angular spectrum of protons, emitted in all AgBr events are obvious:

i) The frequency of protons emitted with small angles is remarkably low.

ii) $dN/d\Omega$ decreases only slightly with increasing emission angle in the interval 20 - 120°.

iii) There is a weak indication of a peak at ~ 45°.

Recent theoretical interpretations have pointed out the possibility of particle emission from the density perturbation fronts, initiated by shock waves in heavy ion interactions [9-11]. In the GeV region, however, it is not clear whether this effect is possible or the transparency of the nucleus is too large. According to the calculations of Greiner et al. [11] a distinct peak at the Mach angle should appear. The only indication of such a peak in our distribution is the small bump at ~ 45°, which is hardly statistically significant. The calculations of Nix et al. [9] take into consideration that the generated shock waves should be curved rather than conical. The result of a calculation performed by J.R. Nix for our experiment is shown in Fig. 12. The overall agreement is weak, but it must be noticed that this preliminary calculation does not take any nuclear transparency into consideration. In the shock wave calculation there is a slight decrease in the particle emission at small angles. It may, however, also be possible to account for this decrease if a cascade, containing a large amount of secondary hadron-hadron collisions, is developed in head on events.

The $d\sigma/d\Omega$ distributions of He nuclei with $E \leq 40$ MeV and $E > 40$ MeV in head on events are shown in Fig. 13. The structure of the spectrum for $E > 40$ MeV is the same as for the total sample (Fig. 9), and this is not surprising since the dominant part of the high energy He nuclei are emitted in events with a large degree of target disintegration.

Multiple production of fast He nuclei is often found. The mean number of fast He nuclei per AgBr event is only 0.75, but nevertheless 60 % of these particles are emitted in events with a multiplicity of three or more such He nuclei. The tendency of a very large fast helium multiplicity in some nucleus-nucleus events was even more pronounced in an earlier investigation with heavier incident nuclei [17].

Owing to the poor statistics of high energy He nuclei, we are unable to conclude whether there is a fine structure in the angular distribution or not. The comparatively constant $dN/d\Omega$ level extended to ~ 90^{o} is noticeable.

It is obvious that statistical models or quasi-elastic scattering between nucleons and alpha clusters in the target nucleus fail to explain the comparatively high degree of isotropy in the emission of high energy He nuclei. Nor can it be yet concluded that shock wave emission is the correct explanation to the problem of the high energy helium emission.

9. Discussion of Results

9.1. ^{16}O-CNO Interactions

In the ^{16}O-CNO interactions at 2 GeV/nucleon we observe that the main structure of the $p_{\perp}$ distribution of He nuclei from the beam nucleus as well as from the target nucleus agrees with a composite Gaussian distribution with $\sigma \approx 140$ MeV/c. The same type of distributions have been found for heavier fragments in other experiments. The frequency of fast He nuclei ($E > 40$ MeV) is very small. These observations seem to support a statistical model with small correlations among nucleon momenta. We must of course also bear in mind that an alpha particle

model might be relevant since both the incident and the target nucleus (to ~ 90 %) has a four-nucleon configuration. The large cross section of multiple alpha production in ^{16}O-CNO interactions supports the alpha particle model.

The high energy part of the proton emission (E > 40 MeV) cannot be explained by statistical models. The wide $p_\perp$ distribution and the agreement between the high energy part of the $d\sigma/dE$ spectrum and intranuclear cascade calculations strongly indicate that protons are frequently emitted in direct nucleon-nucleon scattering.

9.2. ^{16}O-AgBr Interactions

In ^{16}O-AgBr interactions we observe less satisfactory agreement with present theoretical interpretations than in ^{16}O-CNO interactions.

In peripheral collisions the predominant emission of protons and He nuclei can be explained by intranuclear nucleon-nucleon scattering, followed by evaporation from an excited residual nucleus. With a decreasing impact parameter we find increasing deviations from this "two-step" model. The angular distribution of high energy protons in events where the target nucleus is totally disintegrated into nucleons and alpha particles has a structure which must be explained by other phenomena. The shock wave models may be an explanation of the high energy proton and He emission. However, both the theoretical calculations and the statistics of the experiments have to be improved until the theory of shock wave emission can be confirmed or rejected. The high degree of isotropy and the wide $p_\perp$ distribution of the high energy He nuclei is impossible to interpret

merely by quasi-elastic collisions between nucleons (or alphas) and He clusters. Furthermore, some head-on events produce a large number of high energy He nuclei, thereby indicating a violent breakup of the nuclear surface.

We are grateful to Prof. K. Kristiansson and Dr. I. Otterlund for valuable discussions. We thank Dr. H. Heckman and the operational staff of the Berkeley Bevatron for their assistance during the exposure of the emulsion stack. Thanks are also due to Research Engineer B. Lindkvist and her staff for the processing and scanning of the emulsions. The research reported here has been sponsored by the Swedish Atomic Research Council, which is gratefully acknowledged.

Appendix 1

A dip angle correction of the gap density measured on the projected image of a track in the emulsion plane is possible to make if we assume that all grains forming the track are spherical.

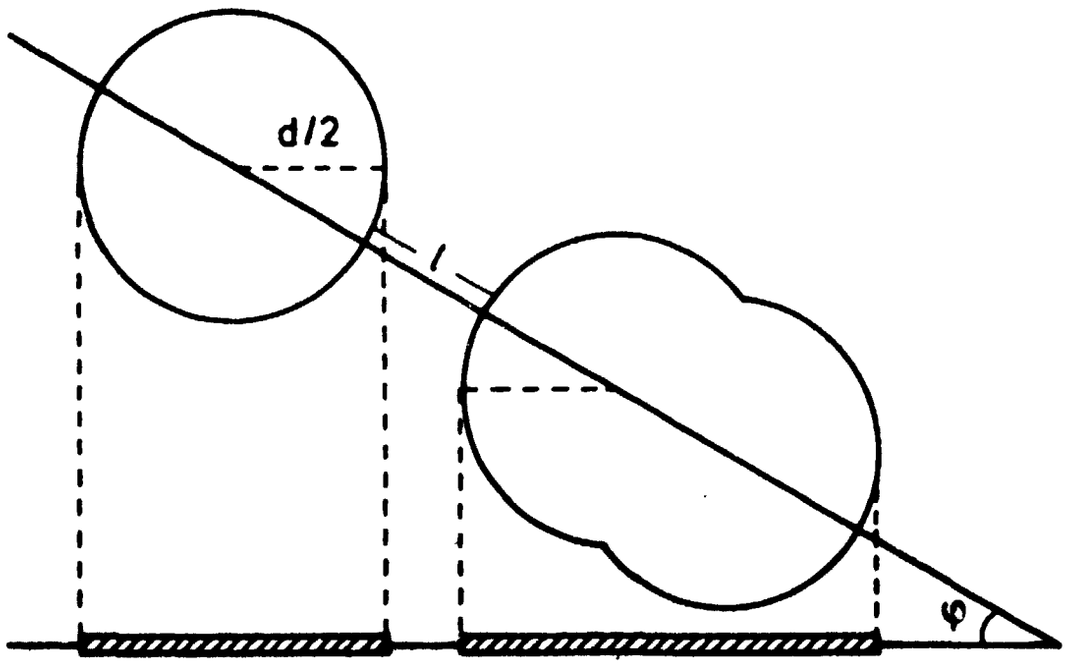

d = The grain diameter (0.45 μm in K2 emulsion)

ℓ = Length of a gap

φ = The dip angle in the undeveloped emulsion

If a gap should be visible in the projected track, the gap length must fulfil the condition: $\ell > (k+d)/\cos\varphi - d$ where k = the smallest visible gap length (0.2 μm in our measurements).

The gap length distribution is exponential:

$$N(>\ell) = N_0 \cdot \exp(-g\ell)$$

where $N(>\ell)$ is the density of gaps with a length $> \ell$,

N_0 is the total gap density and

g is the gap length coefficient, which can be related to $N(>k)$ using calibration tracks with small dip angles. (g = the inverse mean gap length).

The density of visible gaps of a plane track G_0 is as follows:

$$G_0 = N(>k) = N_0 \exp(-gk) \quad .$$

The density of visible gaps in a track with a dip angle φ, (G_φ), is:

$$G_\varphi = N(> (k+d)/\cos\varphi - d)/\cos\varphi = N_0/\cos\varphi \cdot \exp(g(d-(k+d)/\cos\varphi)).$$

This gives the relation between the measured gap density of a plane track and a track with $\varphi > 0$:

$$\boxed{G_\varphi = G_0/\cos\varphi \cdot \exp(g(k+d)(1-1/\cos\varphi)).}$$

Appendix 2

Since only tracks with dip angles $\leq 40^{\circ}$ have been identified with respect to charge and energy, we have to introduce a geometrical correction. An accurate correction can be made since the dip angle interval $\varphi \leq 40^{\circ}$ covers more than 44 % of each emission angle interval. All tracks with dip angles $> 40^{\circ}$ have been registered and the energy loss near the star has been estimated by gap counting (Appendix 1). Consequently, we can control the total dip correction by comparing the registrated number of tracks with the number derived according to the correction.

General correction formula

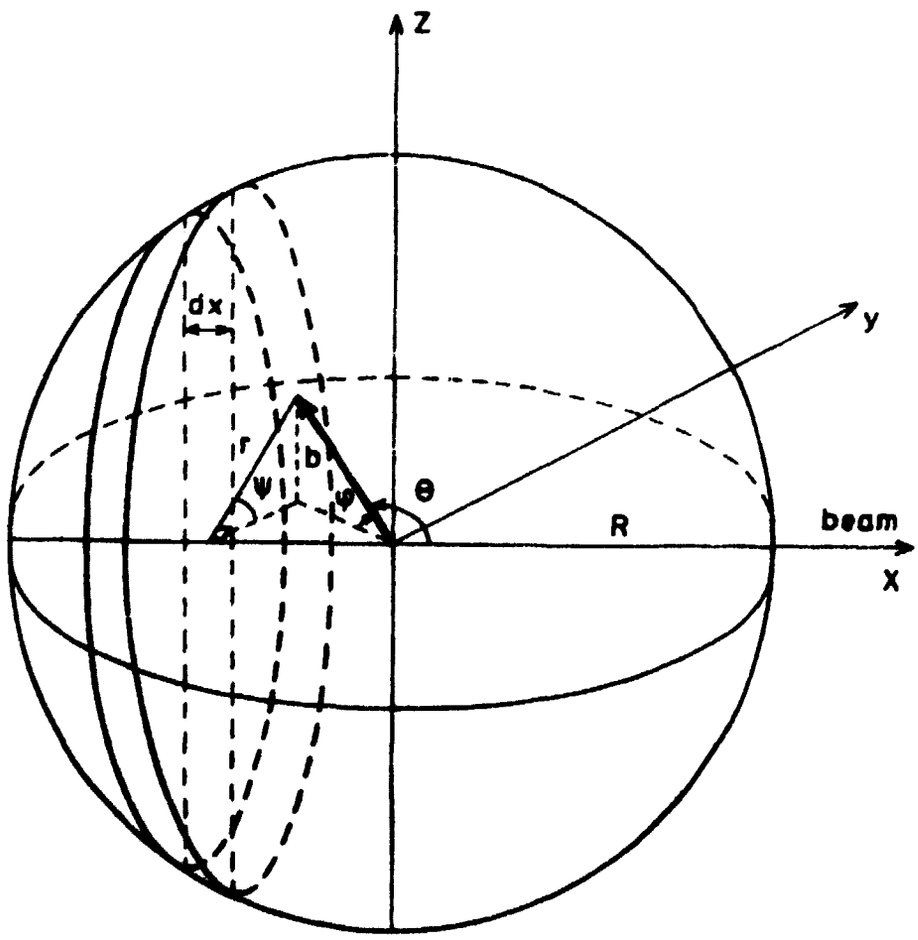

All tracks with dip angles $< \varphi_\ell$ have been measured. Consequently, the distribution of particles with emission angles, θ, in the intervals $0 \leq \theta \leq \varphi_\ell$ and $(\pi - \varphi_\ell) \leq \theta \leq \pi$ is complete. Particles emitted in these angular intervals have therefore been assigned the weight $W = 1$. In the residual angular interval, $\varphi_\ell < \theta < \pi - \varphi_\ell$, the identified particles with $\varphi < \varphi_\ell$ are given a weight $W(\theta) > 1$. We have here disregarded the dip angle of the beam track since this angle is always $< 1^0$.

According to the figure:

$$x = R \sin\theta \text{ and } b = R \sin\varphi$$

The dip angle φ_ℓ corresponds to the Ψ value:

$$\Psi_\ell = \arcsin(\sin\varphi_\ell/\sin\theta) \qquad (\text{since } \Psi = \arcsin \tfrac{b}{r}).$$

$$W(\theta) \cdot 2\pi R dx \cdot 2\Psi_\ell/\pi = 2\pi R dx$$

$$W(\theta) = \pi/2 \cdot \Psi_\ell^{-1}$$

$$\boxed{W(\theta) = \pi/2 \cdot (\arcsin(\sin\varphi_\ell/\sin\theta))^{-1}}$$

REFERENCES

1. Feshbach, H. and Huang, K., Phys. Letters 47B, 300 (1973).

2. Goldhaber, A.S., Phys. Letters 53B, 306 (1974).

3. Hüfner, J., Schäfer, K. and Shürmann, B., Preprint, Heidelberg (1975).

4. Barshay, S., Dover, C.B. and Vary, J.P., Phys. Letters 51B, 5 (1974).

5. Karol, P.J., Phys. Rev. C11, 1203 (1975).

6. Fäldt, G. and Gislén, L., Preprint, Lund 1975.

7. Jakobsson, B., Kullberg, R. and Otterlund, I., Z. Physik A272, 159 (1975).

8. Tolstov, K.D., JINR P1-8662 (1975).

9. Amsden, A.A., Bertsch, G.F., Harlow, F.H. and Nix, J.R., Phys. Rev. Letters 35, 905 (1975).
Nix, J.R., Private Communication.

10. Sobel, M.I., Siemens, P.J., Bondorf, J.P. and Bethe, H.A., Preprint, Copenhagen (1975).

11. Baumgardt, H.G., Schott, J.U., Sakamoto, Y., Schopper, E., Stöcker, H., Hofmann, J., Scheid, W. and Greiner, W., To be published in Z. Physik.

12. Barkas, W.H., Nuclear Research Emulsions I. Academic Press, New York/London (1963).

13. Jakobsson, B., Kullberg, R. and Otterlund, I., Preprint, Lund (1975).

14. Heckman, H.H., Perkins, B.L., Simon, W.G., Smith, F.M. and Barkas, W.H., Phys. Rev. 117, 544 (1960).

15. Barkas, W.H., and Berger, M.J., Natl. Acad. Sci. - Natl. Res. Council Publ. 1133, 103 (1964).

16. Hyde, E.K., Butler, G.W. and Poskanzer, A.M., Phys. Rev. C4, 1759 (1971).

17. Jakobsson, B., Kullberg, R. and Otterlund, I., Z, Physik 268, 1, (1974).

18. Barashenkov, V.S., Beliakov, V.A., Glagolev, V.V., Dalkhazhav, N., Yao Tsyng Se, Kirillova, L.F., Lebedev, R.M., Maltsev, V.M., Markov, P.K., Shafranova, M.G., Tolstov, K.D., Tsyganov, E.N. and Wang Shou Feng, Nucl. Phys. 14, 522 (1959/60).

19. Kullberg, R., Otterlund, I. and Resman, R., Physica Scripta 5, 5 (1972).

20. Lindhard, J., Scharff, M. and Schiøtt, H.E., Mat. Fys. Medd. Dan. Vid. Selsk. 33 no. 14 (1963).

21. Bowman, W.W., Lanzafame, F.M., Cline, C.K., Yu-Wen Yu and Blann, M., Phys. Rev. 165, 485 (1968).

22. Sullivan, J.D., Price, P.B., Crawford, H.J. and Whitehead, M., Phys. Rev. Letters 30, 136 (1973).

23. Greiner, D.E., Lindstrom, P.J., Heckman, H.H., Bruce Cork and Bieser, F.S., Lawrence Berkeley Laboratory Report LBL-3651 (1975).

24. Lindstrom, P.J., Greiner, D.E., Heckman, H.H., Bruce Cork and Bieser, F.S., Lawrence Berkeley Laboratory Report, LBL-3650, (1975).

25. Heckman, H.H., Greiner, D.E., Lindstrom, P.J. and Shwe, H., Proc. 14th Int. Cosmic Ray Conf., München 1975.

26. Judek, B., Proc. 14th Int. Cosmic Ray Conf., München 1975.

27. Lindstrom, P.J., Greiner, D.E., Heckman, H.H., Bruce Cork and Bieser, F.S., Proc. Int. Cosmic Ray Conf., München 1975.

28. Cheshire, D.L., Huggett, R.W., Johnsson, D.P., Jones, W.V., Rountree, S.P., Verma, S.D., Schmidt, W.K.H., Kurz, R.J., Bowen, T. and Krider, E.P., Phys. Rev. D 10, 25 (1974).

29. Abdo, Kh.M., Dalkhazhav, N., Salomov, D.A., Sun Tsin Yan, G. Ya. et al., JINR P1-7217 (1973).

30. Igo, G.J., Friedes, J.L., Palevsky, H., Sutter, R., Bennett, G., Simpson, W.D., Corley, P.M. and Stearns, R.L., Nucl. Phys. B3, 181 (1967).

31. Coor, T., Hill, D.A., Hornyak, W.F., Smith, L.W. and Snow, G., Phys. Rev. 98, 1369 (1955).

32. Renberg, P.U., Measday, D.G., Pepin, M., Schwaller, P., Favier, B. and Richard-Serre, C., Nucl. Phys. A183, 81 (1972).

33. Metropolis, N., Bivins, R., Storm, M., Turkevich, A., Miller, J.M. and Friedlander, G., Phys. Rev. 110, 185 (1958).

34. Crawford, H.J., Price, P.B., Stevenson, J., and Wilson, L.W., Phys. Rev. Letters 34, 329 (1975).

35. Takibaev, Zh.S., Shalagina, E.V., Amankulova, D.S., Titova, N.S. and Shtern, G.R., Sovj. J. Nucl. Phys. 3, 623 (1966).

FIGURE CAPTIONS

1. The relation between gap density and restricted energy loss in our K2 emulsion stack. The points show the behaviour of one typical calibration proton with a range of 12 mm.

2. Total bloblength distribution (last 95 μm) of stopping tracks with dip angle $\leq 40^{\circ}$. The curves are estimations of the proton distribution (solid curve), and the total hydrogen distribution (dashed curve).

3. Relations between the total bloblength and residual range for protons and He nuclei (experimental), deuterons and tritons (calculated from the proton curve).

4. Range distributions of tracks with R < 50μm separated into two groups ($Z \leq 2$ and $Z \geq 3$).

5. The frequency of interactions where light ($Z \leq 2$) particles with R < 50 μm but no recoil nucleus ($Z \geq 3$) are emitted.

6. Overlap parameter (b) as a function of $A_B^{1/3} + A_T^{1/3}$, ($r_o = 1.25$ fm).

7. Energy distributions of protons (a) and He nuclei (b) in AgBr and CNO events.
The curves in a) show results from intranuclear cascade calculations of p-nucleus reactions at 1840 MeV [33]. The CNO distribution is compared to a calculation for p-Al interactions. The AgBr distribution is compared with an estimated p-Ag curve based on Metropolis calculations [33]. Normalization is made at E = 100 MeV.

8. Angular distributions of protons with E > 40 MeV emitted in AgBr and CNO events.

9. Angular distributions of protons, He- and Li nuclei with E > 40 MeV emitted in AgBr events.

10. Experimental transverse momentum distributions of He nuclei emitted from the beam- and target nucleus in ^{16}O-H, CNO, and AgBr reactions.

11. Transverse momentum distributions of protons emitted from AgBr and CNO nuclei.

12. Angular distributions of protons with E > 40 MeV emitted in ^{16}O-AgBr interactions with $N_h \geq 28$.

13. Angular distributions of He nuclei, E > 40 MeV and $E \leq 40$ MeV, emitted in ^{16}O-AgBr interactions with $N_h \geq 20$.

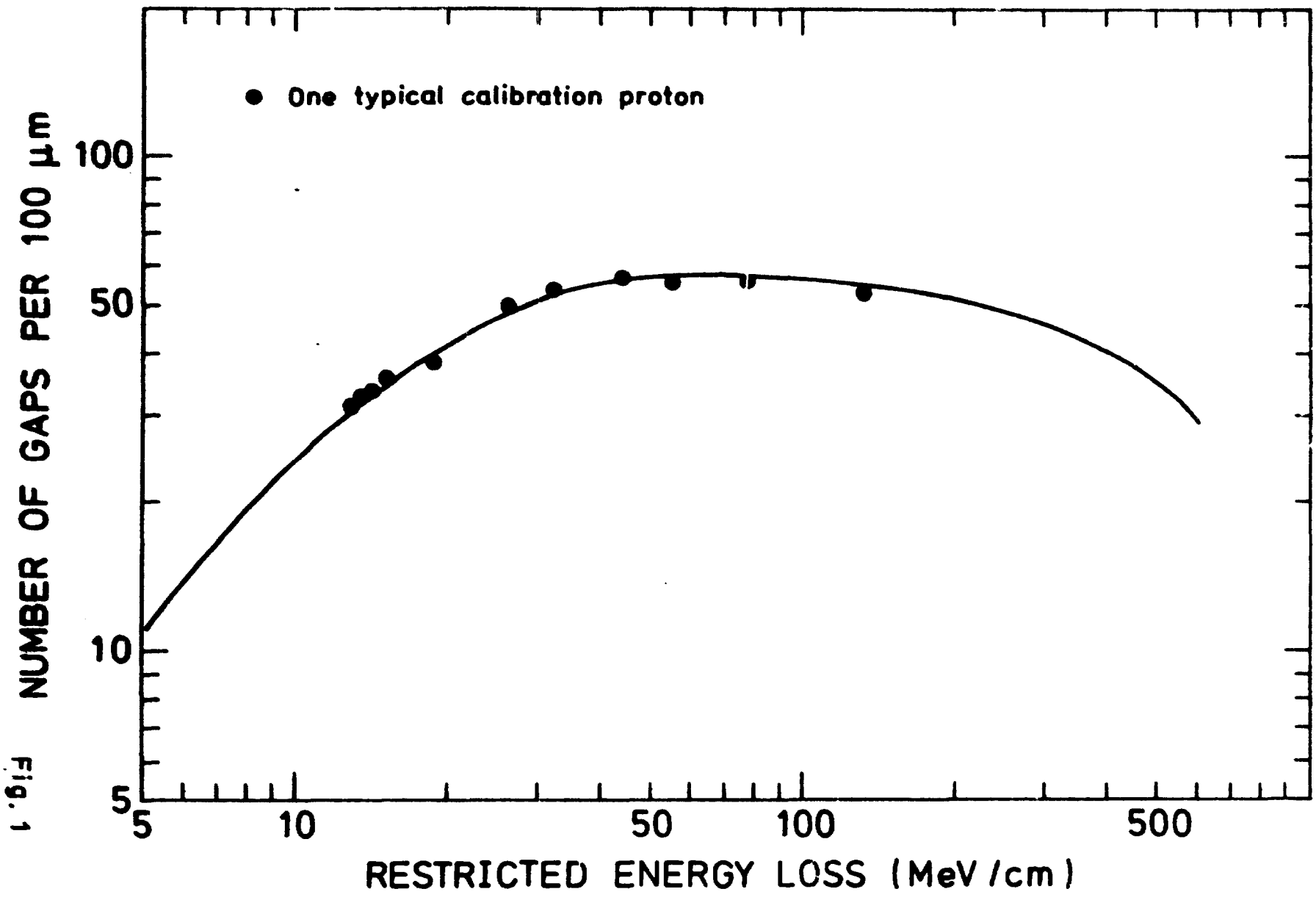
One typical calibration proton
NUMBER OF GAPS PER 100 µm
100
50
10
5
5
10
50
100
500
RESTRICTED ENERGY LOSS (MeV/cm)

Fig. 1

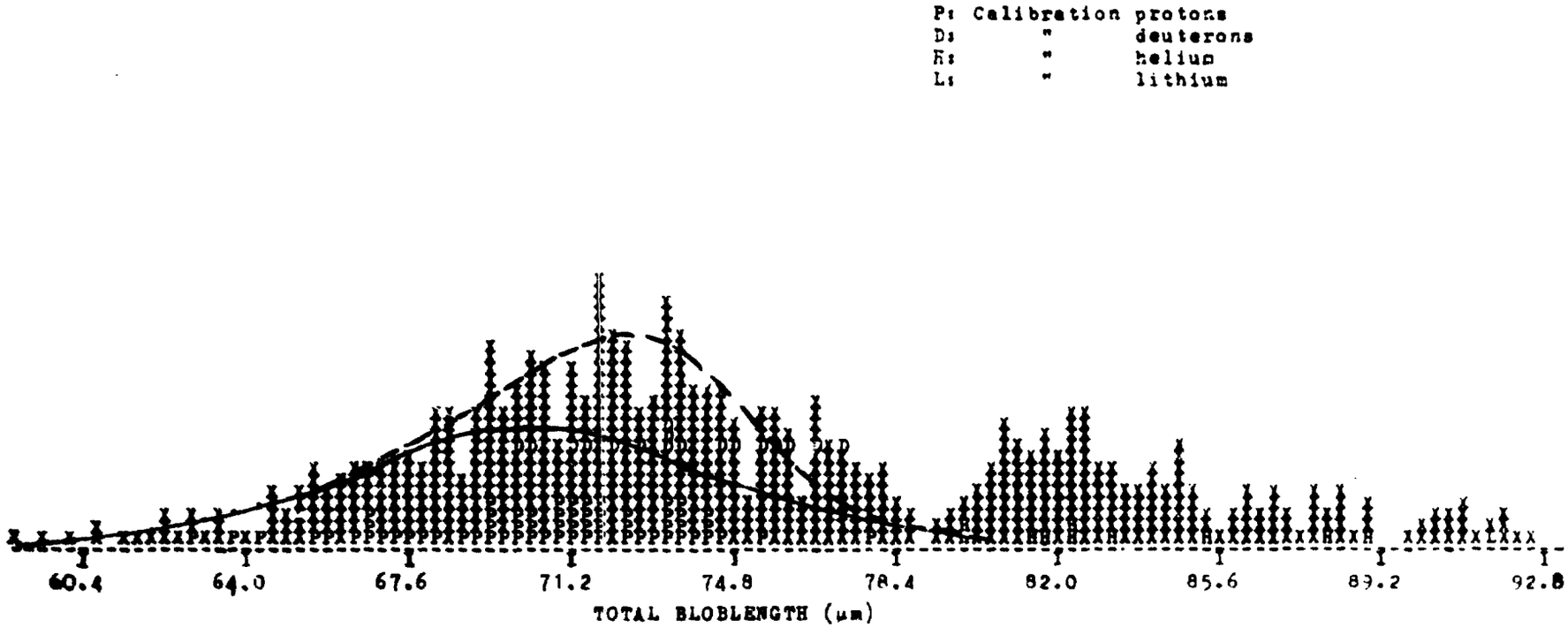
P: Calibration protons
D: " deuterons
H: " helium
L: " lithium
60.4
64.0
67.6
71.2
74.8
78.4
82.0
85.6
89.2
92.8
TOTAL BLOBLENGTH (µm)

Fig. 2

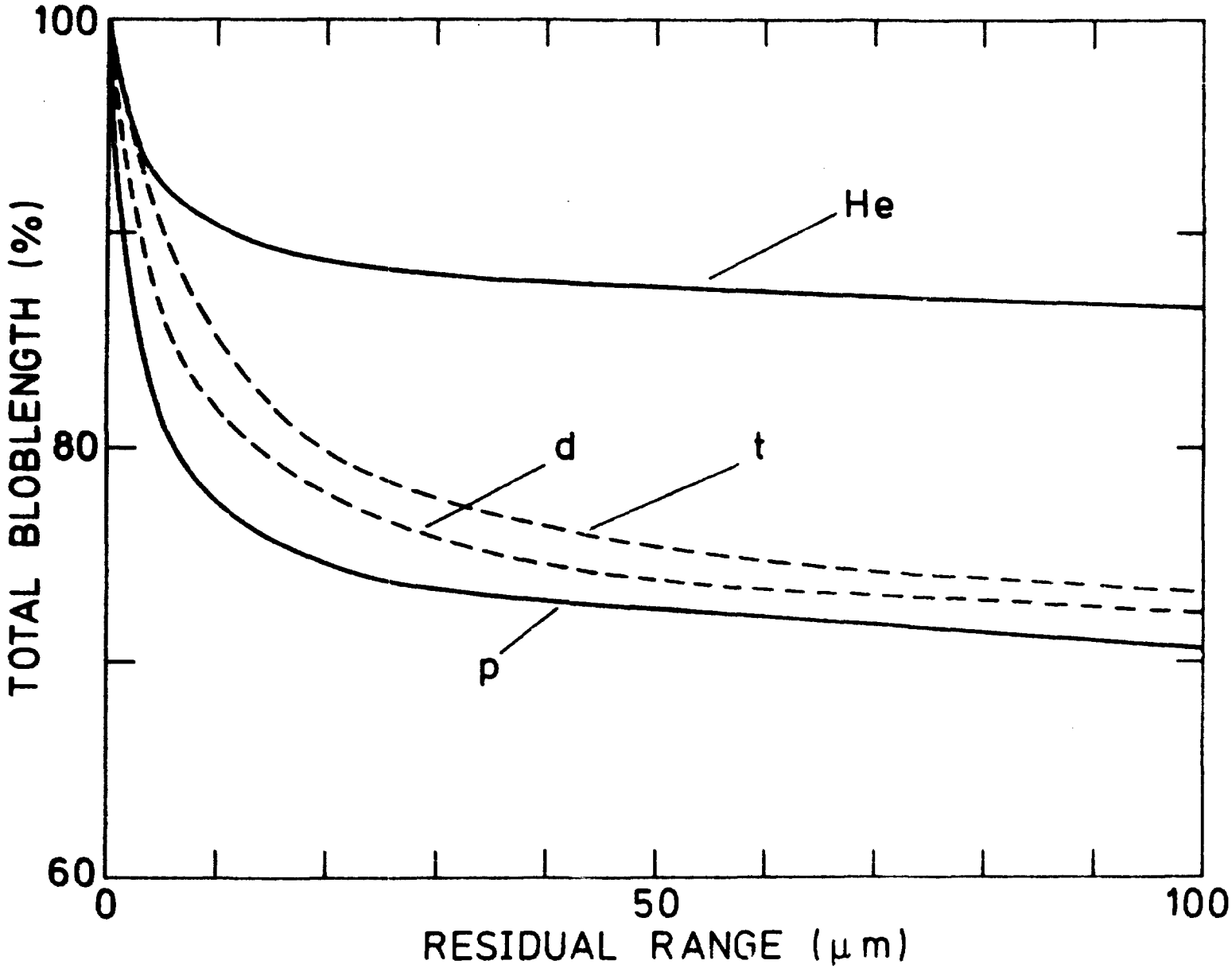

Fig.3

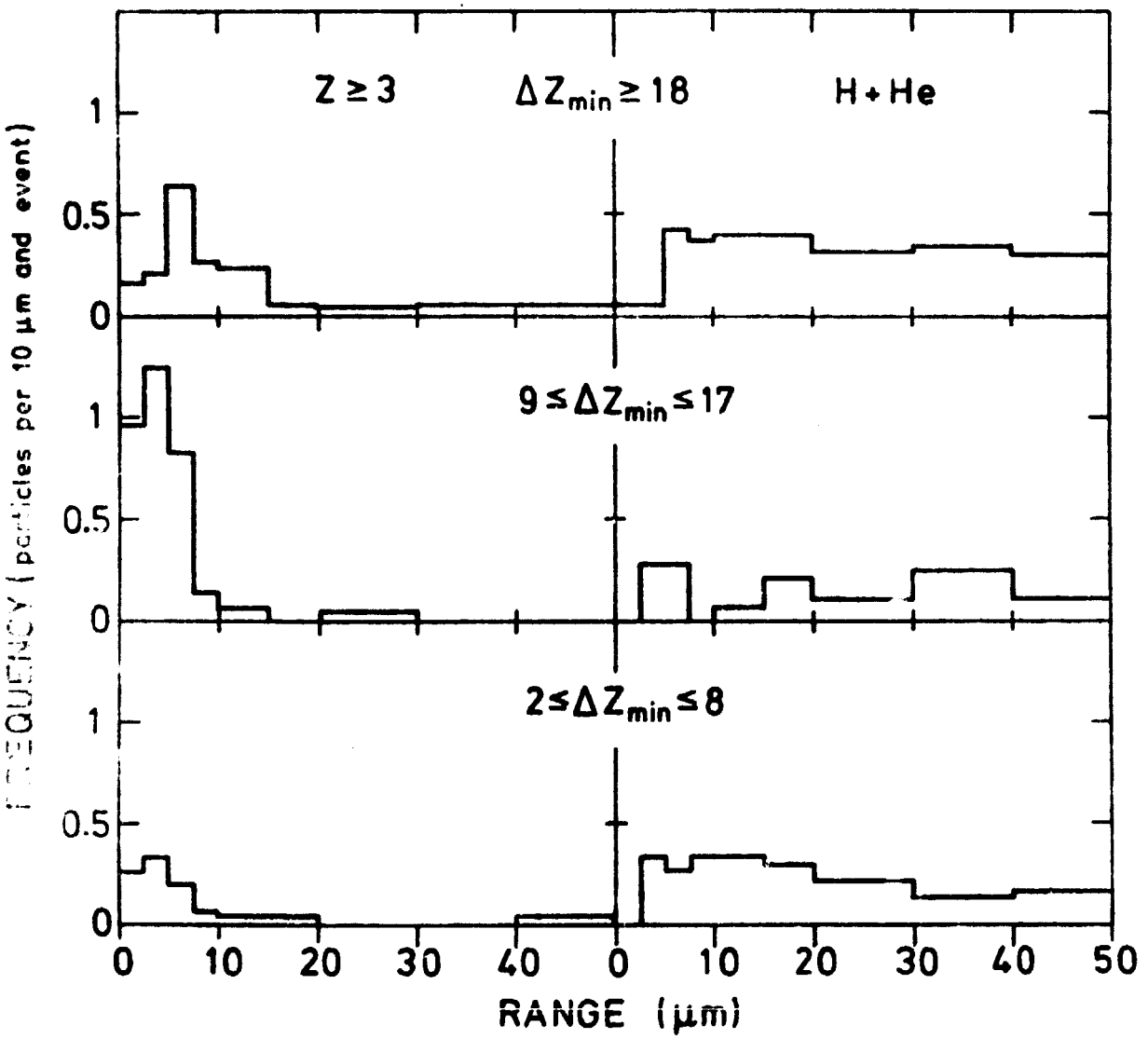
Z ≥ 3
ΔZmin ≥ 18
H + He
9 ≤ ΔZmin ≤ 17
2 ≤ ΔZmin ≤ 8
FREQUENCY (particles per 10 μm and event)
RANGE (μm)
0
0.5
1
10
20
30
40
50

Fig.4

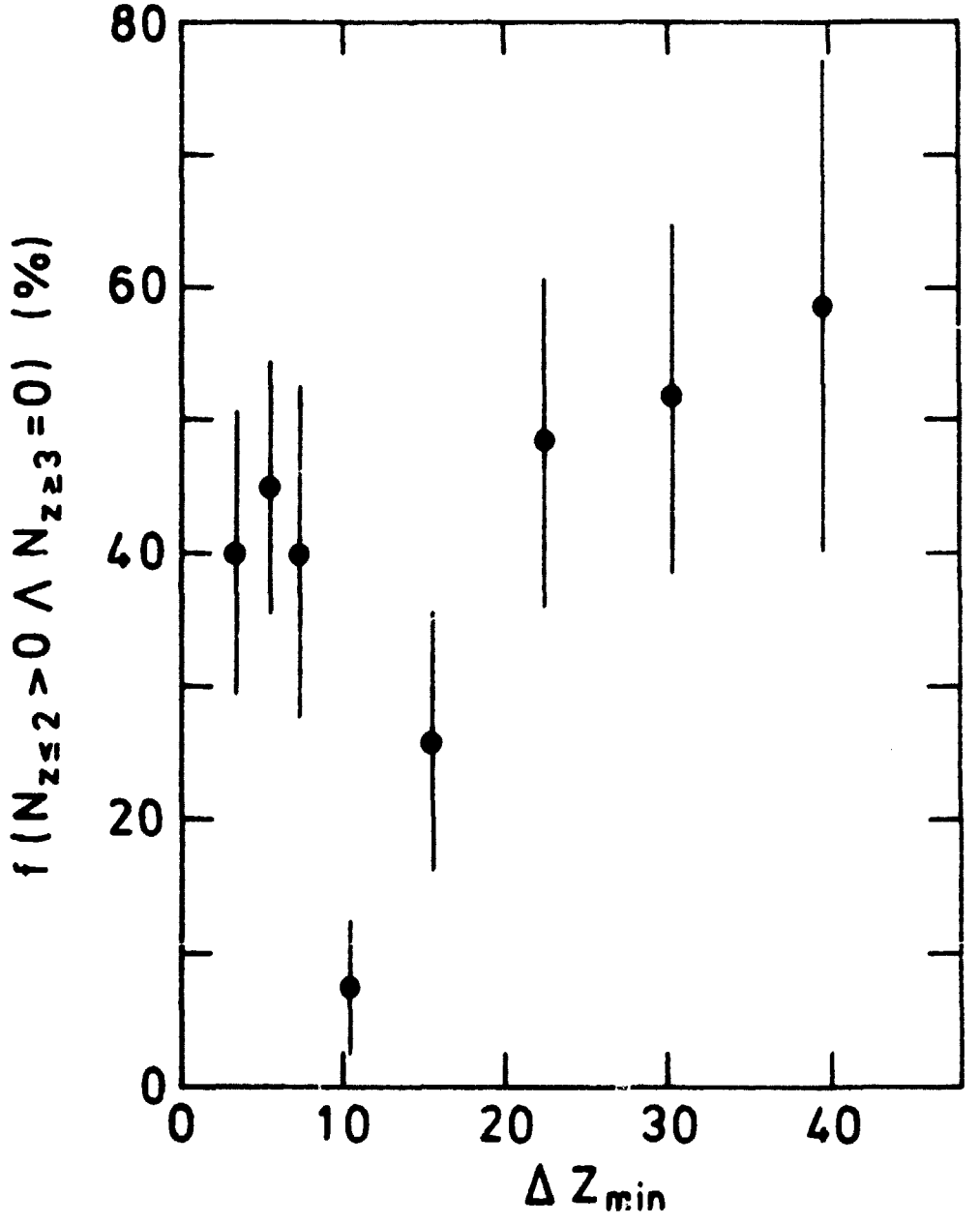

Fig.5

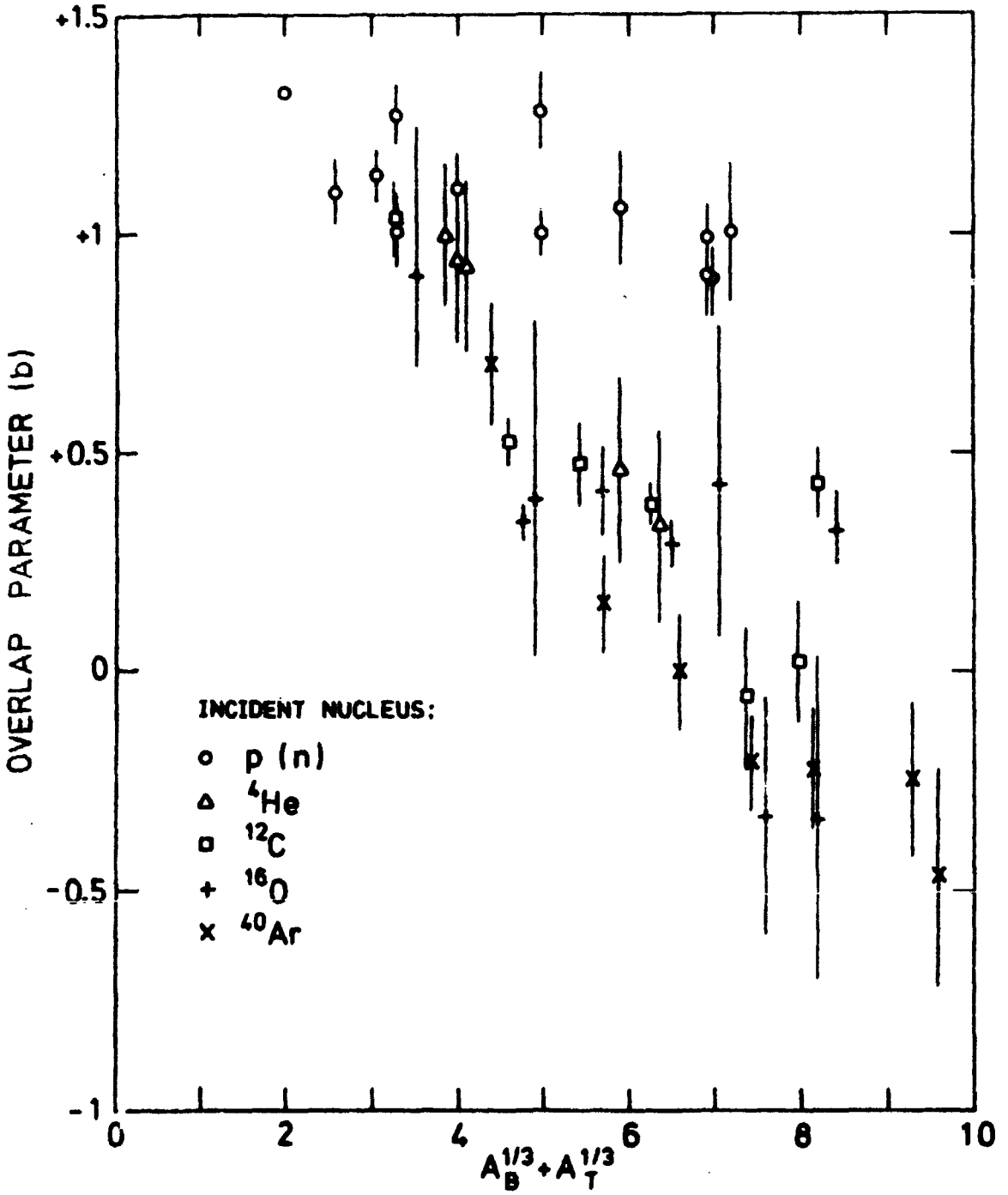
+1.5
+1
+0.5
0
-0.5
-1
OVERLAP PARAMETER (b)
0
2
4
6
8
10
$A_B^{1/3} + A_T^{1/3}$
INCIDENT NUCLEUS:
p (n)
^{4}He
^{12}C
^{16}O
^{40}Ar

Fig. 6

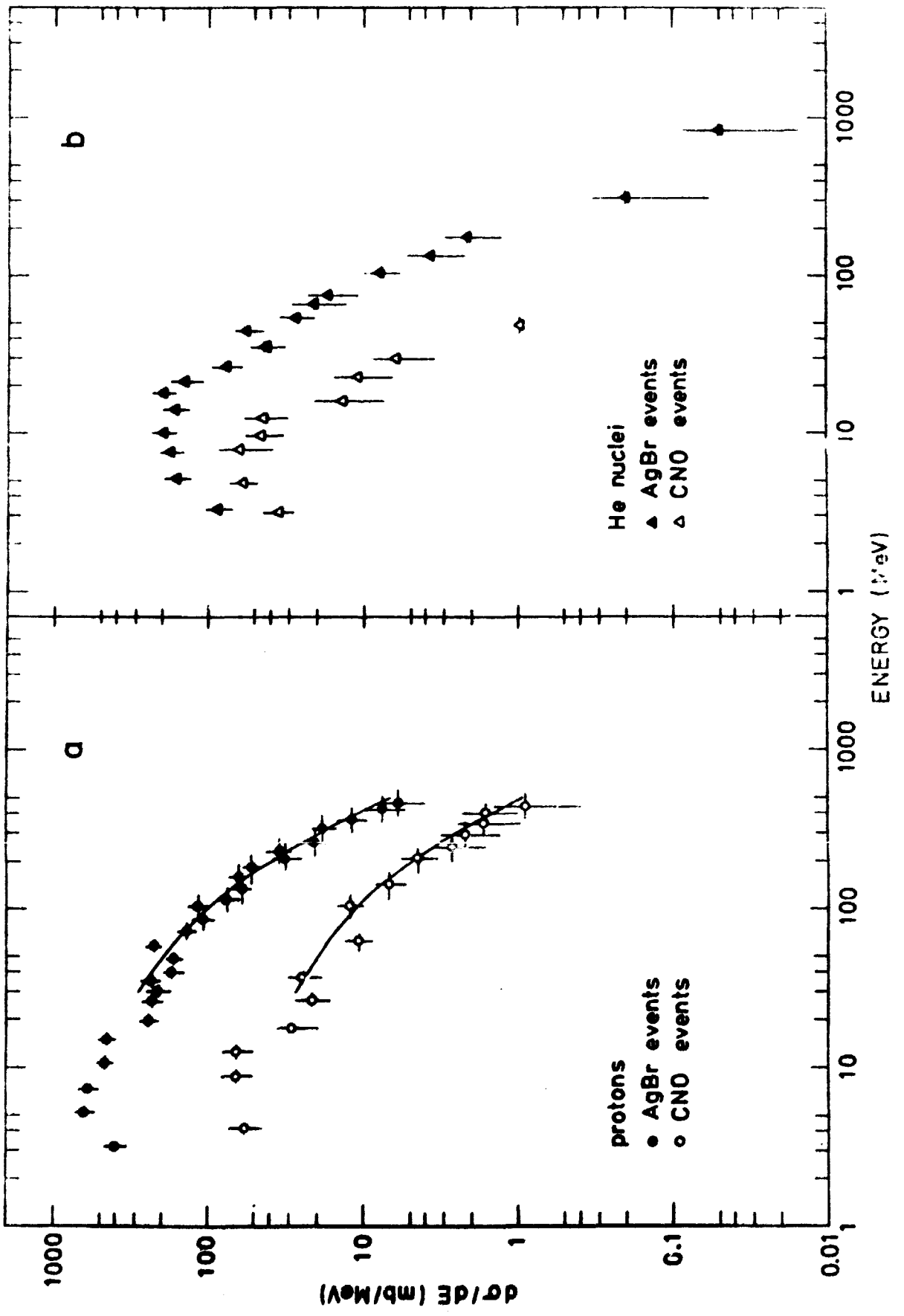
a
b
protons
• AgBr events
○ CNO events
He nuclei
▲ AgBr events
△ CNO events
dσ/dE (mb/MeV)
ENERGY (MeV)
1000
100
10
1
0.1
0.01
1
10
100
1000

Fig. 7

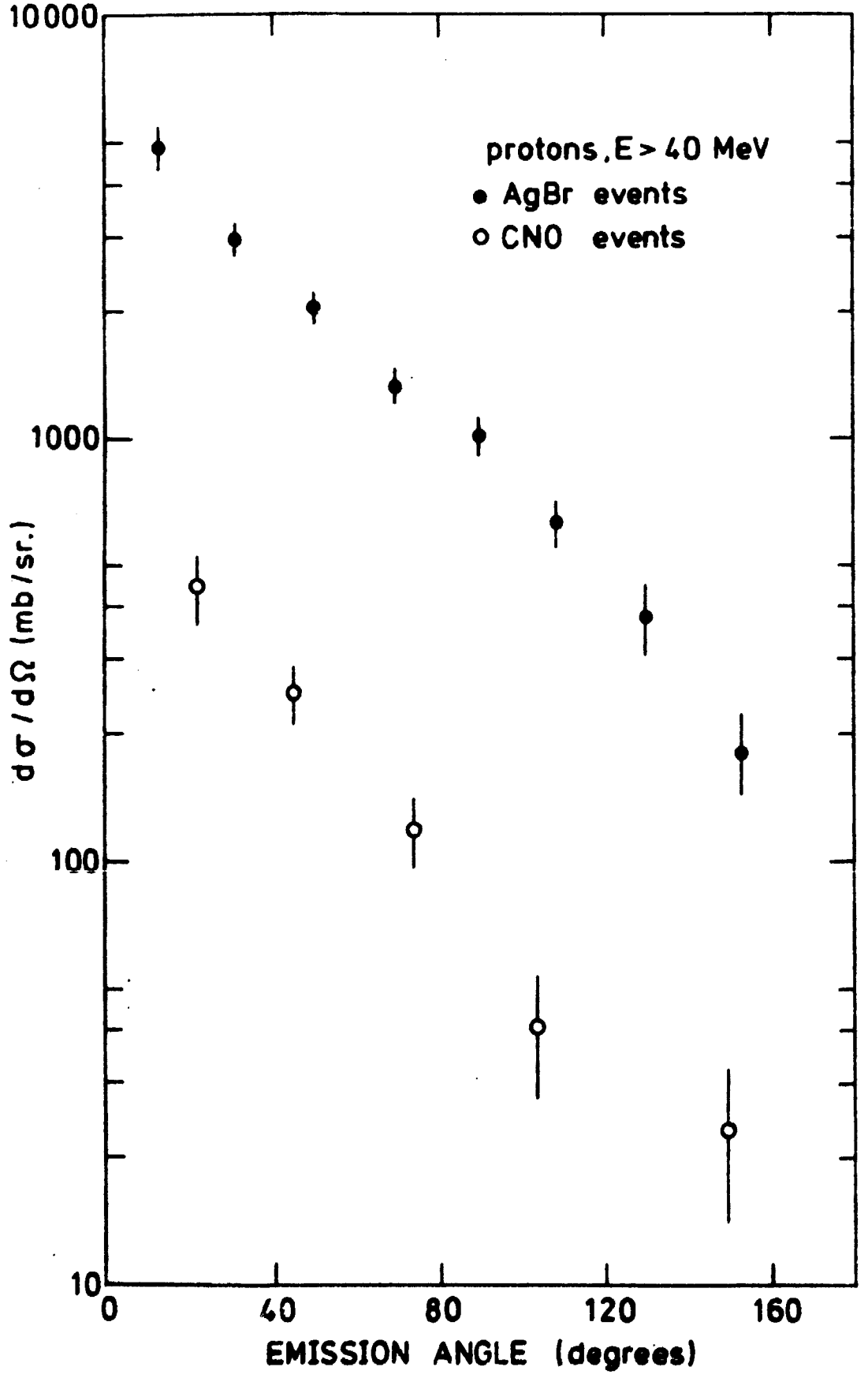
10000
1000
100
10
protons, E > 40 MeV
• AgBr events
○ CNO events
dσ / dΩ (mb/sr.)
0
40
80
120
160
EMISSION ANGLE (degrees)

Fig. 8

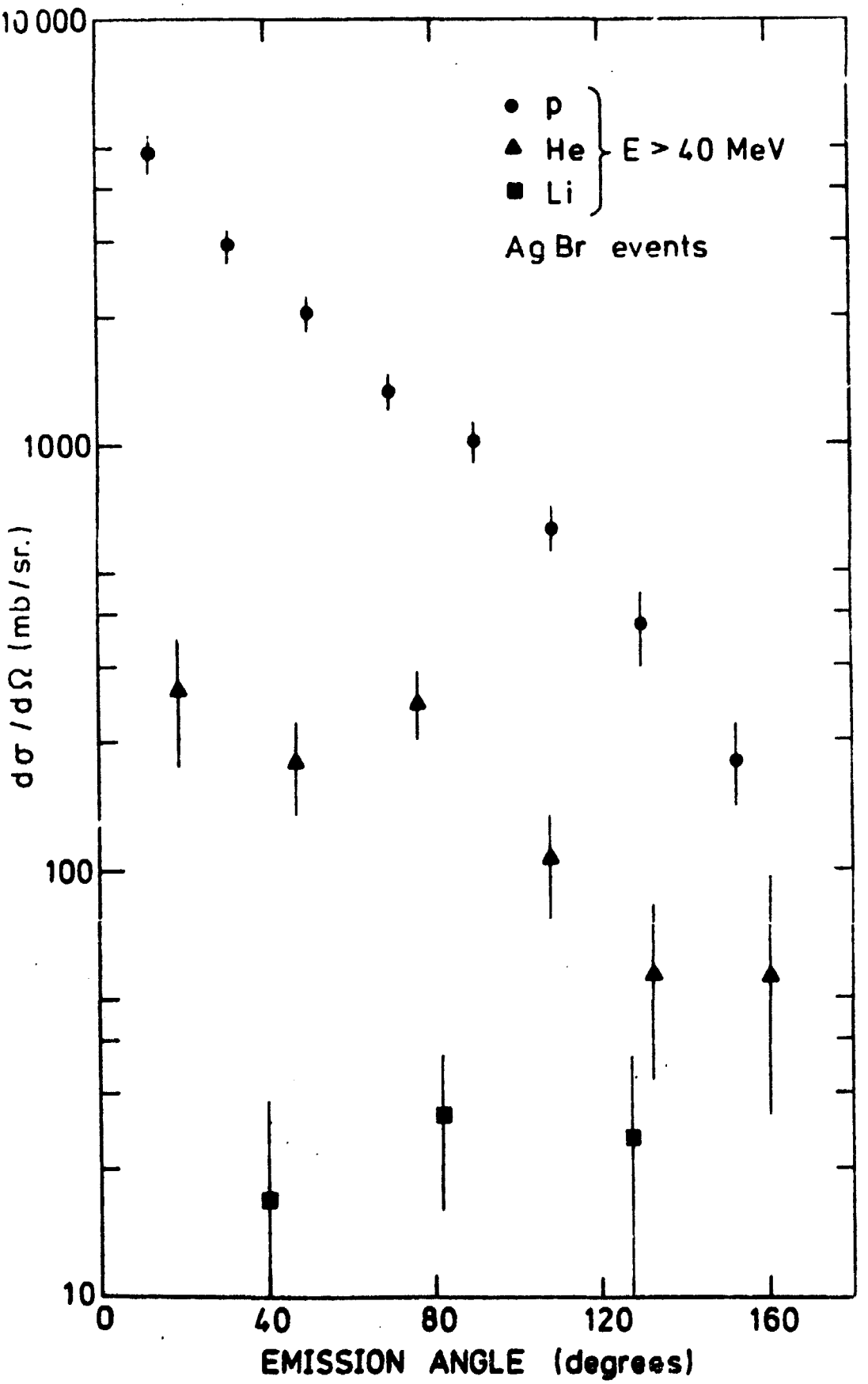
10 000
1000
100
10
dσ / dΩ (mb/sr.)
p
He
Li
E > 40 MeV
Ag Br events
0
40
80
120
160
EMISSION ANGLE (degrees)

Fig. 9

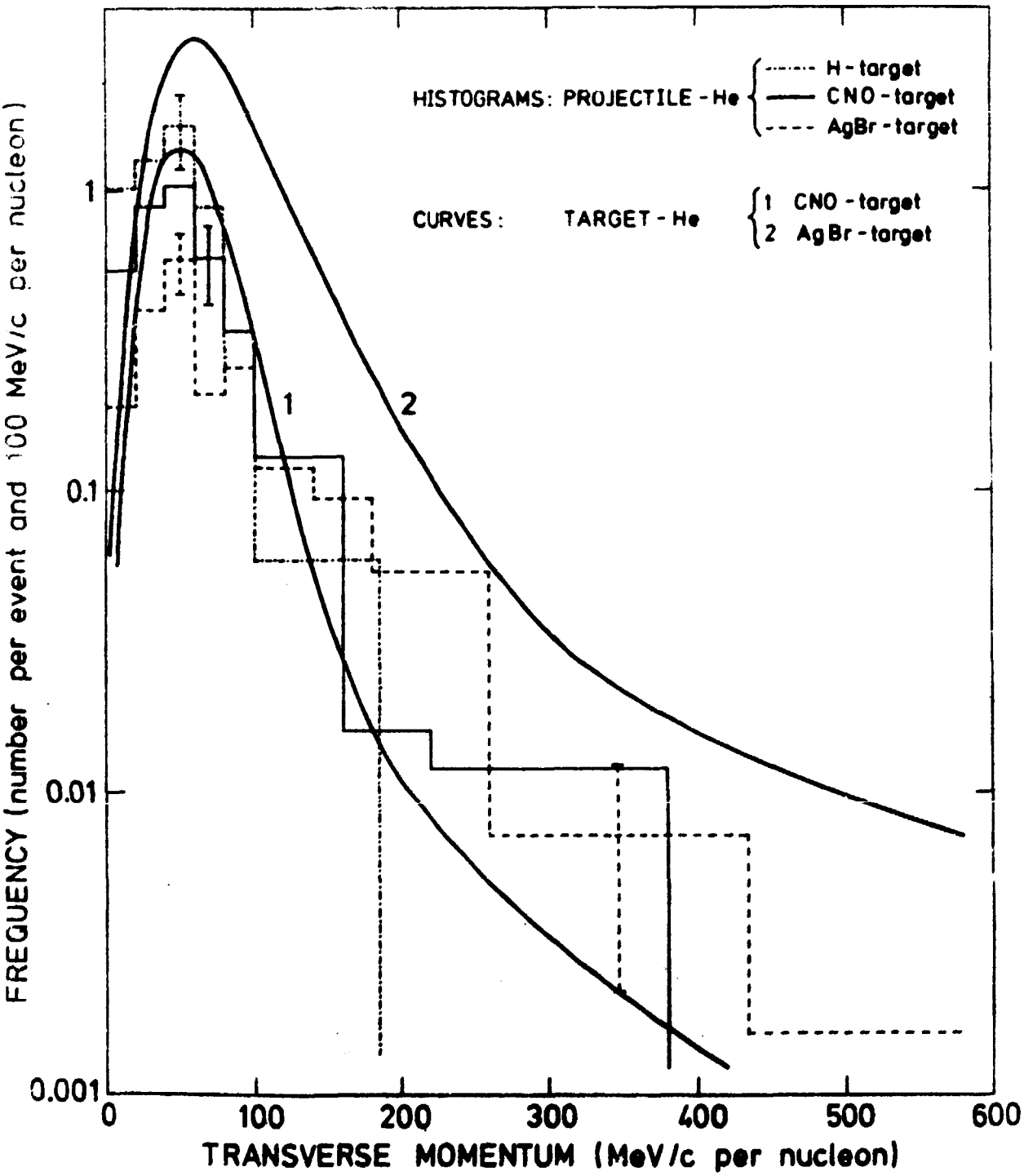
HISTOGRAMS: PROJECTILE - He
H - target
CNO - target
AgBr - target
CURVES: TARGET - He
1 CNO - target
2 AgBr - target
1
2
FREQUENCY (number per event and 100 MeV/c per nucleon)
1
0.1
0.01
0.001
0
100
200
300
400
500
600
TRANSVERSE MOMENTUM (MeV/c per nucleon)

Fig. 10

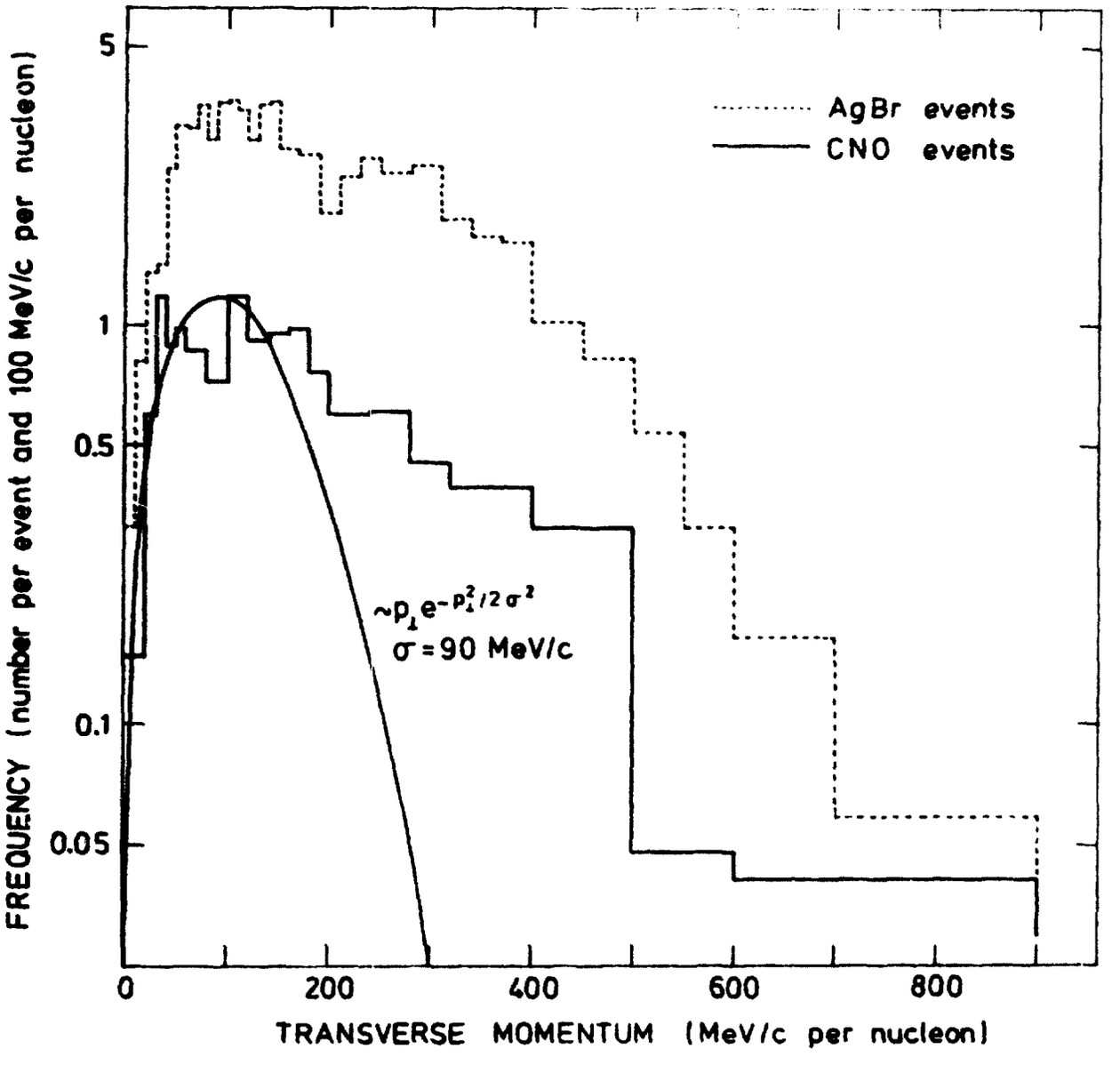
AgBr events
CNO events
$\sim p_\perp e^{-p_\perp^2/2\sigma^2}$
$\sigma = 90$ MeV/c
FREQUENCY (number per event and 100 MeV/c per nucleon)
TRANSVERSE MOMENTUM (MeV/c per nucleon)
5
1
0.5
0.1
0.05
0
200
400
600
800

Fig. 11

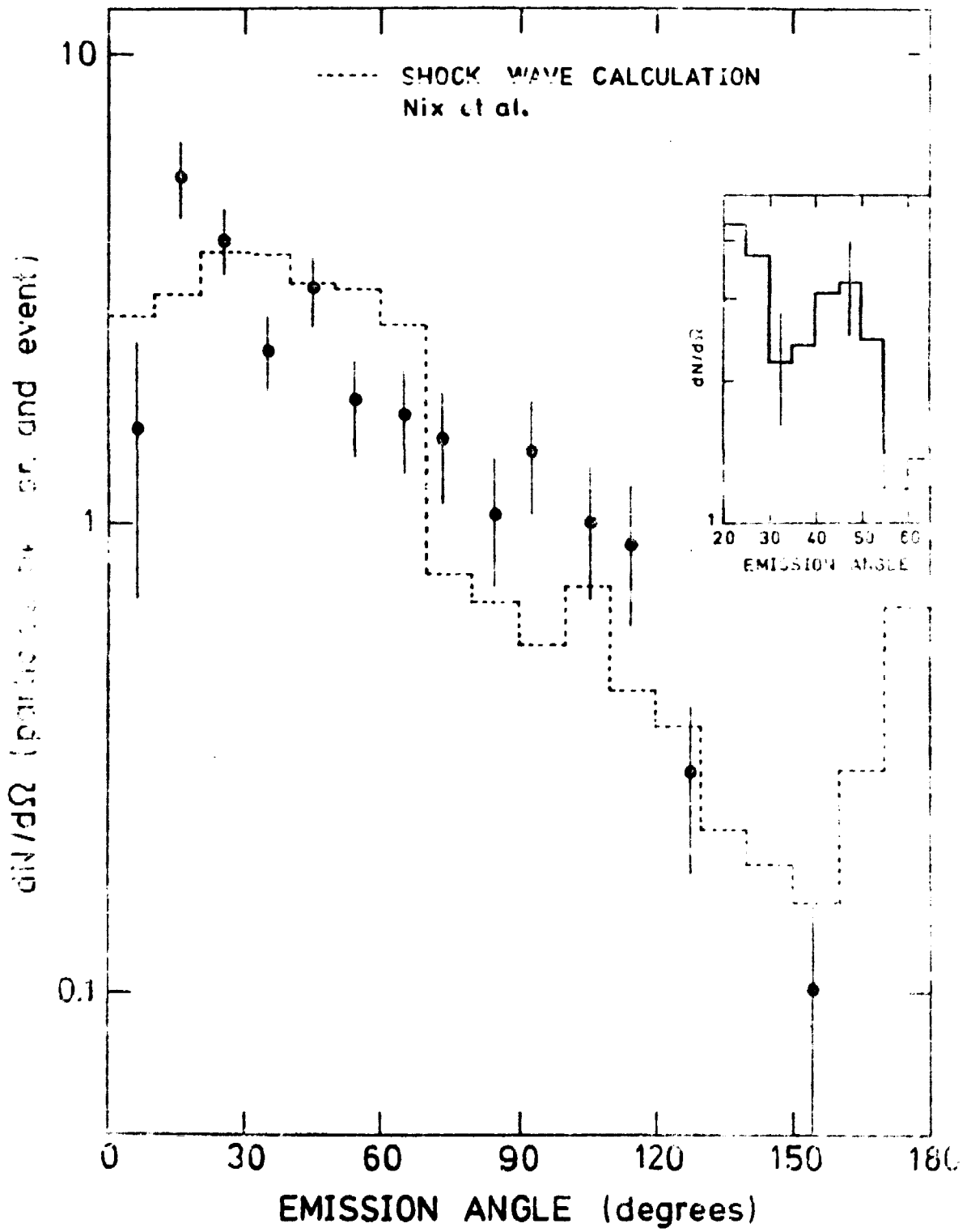
SHOCK WAVE CALCULATION
Nix et al.
10
1
0.1
0
30
60
90
120
150
180
EMISSION ANGLE (degrees)
dN/dΩ (particles per sr and event)
dN/dΩ
20 30 40 50 60
EMISSION ANGLE

Fig.12

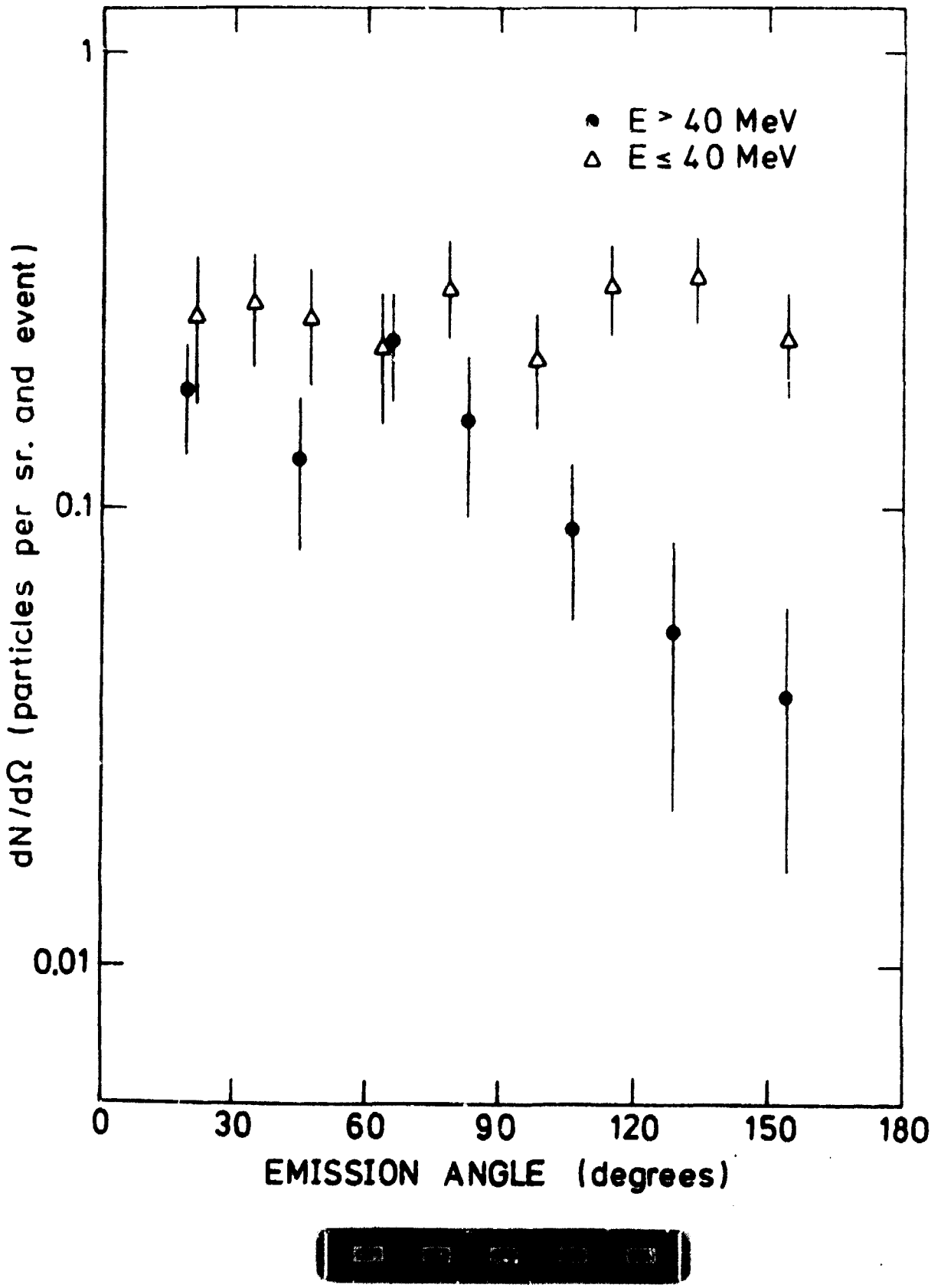
1
0.1
0.01
dN/dΩ (particles per sr. and event)
E > 40 MeV
E ≤ 40 MeV
0
30
60
90
120
150
180
EMISSION ANGLE (degrees)

Fig.13